The Thesis Committee for Vladimir M. Rabinovich

Certifies that this is the approved version of the following thesis:

Pore Pressure and Fracture Pressure Prediction of

Deepwater Subsalt Environment Wells in Gulf of Mexico

APPROVED BY

SUPERVISING COMMITTEE:

Supervisor: _____

Kenneth Gray

_____

Pavel Syngaevsky

Pore Pressure and Fracture Pressure Prediction of Deepwater Subsalt Environment Wells in Gulf of Mexico

by

Vladimir M. Rabinovich, BS PE

Thesis

Presented to the Faculty of the Graduate School of

The University of Texas at Austin

In Partial Fulfillment

of the Requirements

for the Degree of

Master of Science in Engineering

The University of Texas at Austin

August 2011

Dedication

To my family and friends.

Acknowledgements

First and foremost, I would like to give my sincere thanks to my supervisor, Dr. Kenneth Gray, for his continued support and supervision during the course of my academic career. I am very grateful for being given the opportunity to revitalize my academic career, be part of this project, and continuously further my knowledge.

I want to offer my deepest gratitude to Pavel Syngaevsky, who not only served as my co-supervisor, but also encouraged and challenged me throughout my internship and project at Newfield Exploration. None of this would have been possible without his help.

I would like to acknowledge Newfield Exploration for giving me the software and data to be able to complete this project. Newfield Exploration provided an immense working environment with great experiences that I will not forget.

My best wishes and thanks to my office colleague and friend, Xiaoyan Shi, who often enlightened and supported me during my two years of study.

Finally, I would not have been able to accomplish any of this without the continued love and support from my family, especially my father.

Abstract

Pore Pressure and Fracture Pressure Prediction of

Deepwater Subsalt Environment Wells in Gulf of Mexico

Vladimir M. Rabinovich, M.S.E.

The University of Texas at Austin, 2011

Supervisor: Kenneth Gray

There are many complications associated with abnormally high fluid pressures in overpressured formations. Pore pressure can directly influence all parts of operations including drilling, geological studies, completion, and production. Accurate predictions of pore pressure and fracture pressure are vital aspects to the production and completion of safe, time efficient, and cost efficient projects. Knowledge of pressure distribution in the formation can greatly reduce complexities associated with drilling and completing a well.

A three-method pore pressure and fracture pressure study was performed on two prospect deepwater wells located in the Gulf of Mexico. More than thirty offset wells in the greater region were initially analyzed for similarities with the two prospect wells. In the final analysis, only six wells were used to create pore pressure and fracture pressure

models due to inconsistencies in similarities or lack of usable data in many of the offset wells. Pore pressure and fracture pressure models were constructed for the offset wells, and then applied and calibrated for the two prospect wells using drilling data such as mud weights, MDTs (Modular Dynamic Testing), and LOTs (Leak-off Test). Three types of pore pressure and fracture pressure models were used in the study: Eaton's deep resistivity method; Eaton's acoustic sonic method; and Bower's interval seismic velocity method.

Pore pressure and fracture pressure prediction was complicated by abnormal pressure in the formation due to undercompaction and seals. Both prospects were located in a deep subsalt environment. Low permeability and traps prevents fluid from escaping as rapidly as pore space compacts thus creating overpressure. Drilling through salt in deep water is expensive and risky. Elevated pore pressure and reduced fracture pressure underneath salt seals can create very tight mud weight windows and cause many drilling problems, as seen in the results of the offset wells' pore pressure and fracture pressure models.

Results indicate very small pore pressure and fracture pressure windows, or mud weight windows, because of overpressures in the formation caused by such a deep subsalt environment. Many casing points were needed in the final casing design of prospect wells to accommodate the smaller mud weight windows. Pore pressure has the most significant increase immediately below the salt, while the mud weight window remained constant or decreased with depth. The average mud weight window ranged between 1 to 2 pounds per gallon below the salt.

Table of Contents

List of Tables

List of Figures

List of Equations

CHAPTER 1: INTRODUCTION

Pore pressure, or the pressure of fluids within the pores of a formation, is an important assessment that must be carefully made when planning a drilling project. Formations with pressures higher than hydrostatic pressure can be encountered in varying areas and depths. Being unaware of areas with overpressures can create many potentially catastrophic events such as blown reservoir seals, drilling fluid losses, or formation fluid influxes. There are many causes of overpressure; thus, it is vital to take the time to strategically plan, analyze, and model pore pressures and fracture pressures as accurately as possible.

1.1 Background

Hydrostatic pressure, or normal pressure, refers to formation pressures which are equal to the hydrostatic head of a column of water of equal depth. Sedimentary rocks maintain hydrostatic pressure if the fluid within their pore space is allowed to escape as sediment compacts. Typical values of hydrostatic pressure gradients range from 0.433 psi/ft in fresh water to 0.465 psi/ft in salt water. Hydrostatic pressure is affected by the temperature of the column and the concentration of salts and gasses in the fluid column. The higher the salt concentration in the column, the higher the hydrostatic pressure will be.

Overpressure is the amount of pore pressure that exceeds the hydrostatic pressure. The overburden stress is a typical upper limit for pore pressure and pressures in this range are dangerous. Shales are the preferred lithology for pore pressure and fracture pressure

predictions because they are the most responsive rock types to abnormal pressures. The causes of overpressure can be broken down into four categories: undercompaction, lateral transfer, tectonic loading, and fluid expansion.

Undercompaction is the most common cause of overpressure and occurs when formations prevent pore fluids from escaping as rapidly as the formation compacts. The excess pressure builds up as pore space tries to compact and the weight of newly deposited sediments compresses the fluid. In many cases, an impermeable seal, such as a salt trap, would cause the pressure of an impermeable fluid to increase at the same rate as the overburden stress. Tectonic loading is similar to undercompaction; that is, it squeezes trapped pore fluids due to tectonically driven stresses and creates overpressure. However in many cases, the overpressure caused by tectonic loading is much greater than that of undercompaction.

Fluid expansion can occur when pore fluids are heated up, hydrocarbon maturation takes place, or formation water expands. Therefore, as the fluid increases in size, overpressure is created. In low permeable layers, very high overpressures can be created. The overpressure due to fluid expansion reduces the weight, or load, being carried by the grains. Fluid expansion is one of the few causes of overpressure that can decrease effective stress. Another type of overpressure can result when fluids are driven from a higher-pressured zone to a lower-pressured zone; this is known as lateral transfer. A lateral transfer usually occurs in dipping layers and faults, which can drive pore fluids updip and transmit pressure into sands.

1.2 Literature Review

The majority of the world's hydrocarbons have been generated in seal-bound compartments from source rocks. The migration of this oil is a pressure driven process which is controlled by the pressures inside the fluid compartments. The concept that oil is originated in fine-grained source rocks and migrates into coarse-grained rocks was first suggested by Munn[1] in 1909 as the hydraulic theory for migration and accumulation of oil.

Sedimentary basins often contain two types of hydrogeological systems: shallow or deep. The shallow systems exhibit normal hydrostatic pressure, while the deep systems often contain fluids at abnormal pressures. The deeper hydrogeological systems contain compartments that are not in hydraulic pressure communication with one another, and therefore exhibit variations in pressures that can pose problems for drillers.

M. King Hubbert[2] was the first to publish a conceptual model for a flow field based on head potential. Hubbert applied ground-water flow techniques to the study of migration in rock formations. Hubbert's model predicted the characteristics of the flow net in both recharge and discharge areas. In 1953, Hubbert[3] published a paper with several findings: subsurface fluids move parallel with bedding from regions of higher fluid potential to regions of lower fluid potential; fluid movement in one aquifer or compartment is independent of fluids in other compartments; and petroleum fluids can be shifted by moving water. However, Hubbert's methods only apply to shallow formations with pressures near hydrostatic pressure.

As drilling projects aimed for deeper and deeper prospects, Hubbert's concepts that suggested pressures were attributed to fluid flow to and from the surface no longer applied to higher pressure formations. In 1959, Hubbert and Rubey[4] suggested that unless the formation is completely impermeable, fluids must always flow away from pressures higher than hydrostatic until the excess pressure is relieved. However, in 1975, Bradley[5] proved that a slow drained mechanism would relieve the overpressure differences in a short period of time. Therefore, in order for a formation to maintain abnormal pressure for a long period of time, the formation must contain a fluid seal.

Stanescu et al.[6] published a case study in 1969 showing data on the Romanian Ernie Dome field. The overpressure field contained a seal at 4,000 ft. The gradient above and below the seal were 0.45 psi/ft, but the pressure at the base of the seal was about 1,600 psi greater than the top of the seal. This field was one of the first examples with abnormal pressure at the base of the seal, while assuming the same gradient above and below the seal.

Many case studies have been done on Cook Inlet, a field in Alaska. Cook Inlet is one of the many fields that exhibit top seals of overpressure starting at depths of around 10,000 ft. North[7] suggested that Cook Inlet is a planar topped seal because it is a fault-bounded depression within a compressional forearc basin. Cook Inlet production occurred in reservoirs immediately above the seal. The maximum gradient in this formation was 0.465 psi/ft, which is slightly higher than the hydrostatic pressure in the area, 0.45 psi/ft.

Once the presence of abnormal pressure is identified, the real challenge lies in modeling formation pore pressure and fracture pressure. The normal compaction trend, described in Chapter 2, is not always uniform and varies with different sedimentary basins. In 1953, Dickinson[8] created a shale porosity-depth relationship for the Gulf Coast Tertiary basin. The curve shows high porosities due to abnormally high fluid pressure. This shows that the Gulf Coast shales have not reached their equilibrium condition of compaction. Based on Dickinson's findings, abnormal pressure exists in shales below 7,000 ft, while shales above 7,000 ft contain hydrostatic pressure.

In 1948, Terzaghi and Peck[9] created a soil-consolidation laboratory model that looked at the compaction phenomena of a water-saturated clay. Terzaghi's used perforated metal plates separated by metal springs in water in a cylindrical tube. The plates simulate the clay, while the springs simulate the contact between clay particles. Terzaghi found that pore pressure can be calculated as the difference between the overburden pressure and the effective pressure. Effective stress is the amount of overburden pressure that is carried by the rock matrix. Terzaghi's model is similar to the work of Hubbert and Rubey[4].

Resistivity logs, sonic logs, neutron logs, and seismic velocities can be used to estimate pore pressure and fracture pressure. The resistivity of shale is affected by salinity, porosity, and temperature. Hottman and Johnson[10] were the first to establish normal compaction trends for Texas and Louisiana fields. In an overpressure area, the values of transit-time deviates from the normal compaction trend, and this deviation is used to calculate the pore pressure. Eaton's[11] method uses the difference in the measured

and estimated normal trend travel times and resistivity values to infer the increased pore pressure. Similarly, Bower's[13] method uses the difference in seismic interval velocity values and normal compaction trend values to estimate the pore pressure.

1.3 Problem Objectives

The objectives of this research is to model pore pressure and fracture pressure for two deepwater prospects and to create the safest and most efficient casing design. The steps taken during the project are as follows:

- Find the most suitable offset wells for Prospect A and Prospect B
- Quality control all the data
- Create overburden gradient using bulk density log
- Identify the shale zones using gamma ray log
- Create normal compaction trends for each method using the shale points for deep resistivity log, sonic log, and seismic interval velocity log
- Estimate pore pressure and fracture pressure for offset wells using Eaton's resistivity and sonic methods
- Calibrate the models using drilling data and compare to original offset data
- Create synthetic bulk density curve for Prospect A and Prospect B using offset wells bulk density for each respective prospect well
- Estimate pore pressure and fracture pressure for prospect wells using Bower's seismic interval velocity method and calibrate the models
- Create safe and efficient mud weight and casing designs for prospect wells

CHAPTER 2: DATA AND PROCEDURE

2.1 Data Available

Initially, more than thirty offset wells were analyzed. The optimum requirements needed to create precise pore pressure and fracture pressure models for offset wells are:

- Location and depth
- Salt seal or subsalt environment
- Gamma ray log, GR
- Deep resistivity log, RDEEP
- Acoustic sonic log, DTCO
- Bulk density log, RHOB
- Modular Dynamic Testing formation pressure points, MDT
- Leak-off test pressure points, LOT
- Mud weight log, MW
- Seismic interval velocities or trace logs

Location and depth were the priority; the two prospect wells are located in a deep, subsalt environment. Offset wells needed to be located in a similar basin type with a salt seal. The three models for pore pressure and fracture pressure created for each offset well required high quality gamma ray logs, deep resistivity logs, and sonic logs. The majority of the offset wells that were not used in the final study lacked certain logs or missed entire sections of logs. Drilling data such as LOT (Leak-off Test) pressure points, MDT

(Modular Dynamic Testing) formation pressure points, and mud weight logs were crucial in calibrating and finalizing pore pressure and fracture pressure models.

Limited data was available for the majority of the wells; those offset wells were not used in the final pore pressure and fracture pressure models. Many offset wells did not meet the requirements needed to create accurate pore pressure and fracture pressure models. Other logs such as rate of penetration, caliper, and density correction benefited the study by allowing the creation of BADHOLE flag curves, or sections of log with faulty data. These sections were quality controlled with a patching function or a synthetic curve generator. Table 1 and Table 2 below show the summary of petrophysical data used to create pore pressure and fracture pressure models for offset wells.

Table 1: Summary of petrophysical data of five offset wells for Prospect A study

	A1	A2	A3	A4	A5
Data Type	TVD Range (ft)	TVD Range (ft)	TVD Range (ft)	TVD Range (ft)	TVD Range (ft)
Gamma Ray	5000 - 29600	4900 - 31100	5100 - 30000	9500 - 22500	4000 - 26500
Density	18000 - 29600	24239 - 30423	18275 - 29800	10750 - 23250	N/A
Resistivity	5000 - 14060 17925 - 29600	4900 - 9724 18000 - 31100	5100 - 9200 13150 - 30000	10850 - 22900	4000 - 26500
Sonic	17950 - 29600	24239 - 30285	17990 - 29773	10800 - 22100	22000 - 26500
Caliper	17903 - 29600	24351 - 30364	18035 - 29960	N/A	N/A
Seismic	5000 - 29600	4900 - 31100	5100 - 30000	9500 - 22500	4000 - 26500

Table 2: Summary of petrophysical data of two offset wells for Prospect B study

Data Type	B1	B2
Gamma Ray	TVD Range (ft)	TVD Range (ft)
Density	4500 - 29663	4300 - 29736
Resistivity	20500 - 29865 4500 - 29663	19500 - 28685 4500 - 28450
Sonic	20500 - 26166	19824 - 27978
Caliper	19191 - 29963	19418 - 28677
Seismic	4500 - 29663	4300 - 29736

2.2 Geological Setting

The geology was dominated by salt tectonics influenced by terrigenous clastic sediments supplied primarily from the Mississippi River. Clastics can create many hydrocarbon reservoirs and seals. Early Miocene sedimentation occurred on unconfined slopes because the salt was not yet deformed. Sediment continued to accumulate in the deep troughs into the middle Miocene, and salt withdrawal began around the minibasins which resulted in anticlines. Late Miocene deposition became more restricted by middle Miocene salt movements. Large growth faults were created as a result in some basins.

Four types of minibasins were observed in the area. The first minibasin is a symmetric salt roller that traps sands from turbidites near depressions. After the salt withdrawal, the depressions become structures that carry sands at the crest. The second minibasin forms on the edge of sloping salt domes. Sands are pinned against the basinward migrating salt and stack in an offset pattern. The third minibasin is a listric growth fault where sands become trapped against the fault on the downthrone side. These sands will downlap in a northerly direction against a salt weld. This was seen for one of

the prospect wells. The fourth minibasin was simply deposited by coarse-grained material due to the reduction in slope gradient.

2.3 Methodology

There are several assumptions that must be made in order to interpret pore pressure and fracture pressure:

- Mechanical compaction is the dominant mechanism for porosity reduction
- Mechanical compaction depends on values of Terzaghi's effective stress
- Compaction is a one-dimensional process
- Overburden can be estimated from bulk density log

The pore pressure and fracture pressure models are based on Terzaghi's effective stress principle which states that pore pressure is the difference between the overburden pressure and the effective stress. Effective stress is the amount of overburden pressure that is supported by the rock matrix.

$$PP = \sigma V - \sigma E \quad (1)$$

Where,

PP = Pore pressure

σV = Vertical stress

σE = Effective stress

2.3.1 Overburden Pressure

Overburden pressure is an important part of the pore pressure and fracture pressure model and must be estimated as carefully as possible. At any depth, the overburden pressure is pressure, or stress, imposed on the layer by the weight of the overlying material. Overburden pressure was calculated using the RHOB log, or bulk density of the formation. Bulk density logs are generally obscured or absent at shallow depths; therefore, it is necessary to perform a density interpolation.

$$RHOB = \rho f + A * (Dbml)B \quad (2)$$

Where,

RHOB = Bulk density, gm/cc

ρf = Fluid density, gm/cc (1.03 gm/cc)

Dbml = Depth below mudline, ft

A = Compaction coefficient

B = Compaction coefficient

2.3.2 Shale Intervals

Shales are the preferred lithology for pore pressure and fracture pressure predictions because they are the most responsive rock types to abnormal pressures. Gamma ray logs and a mud logs are used to select the shale intervals. This was done by creating two cut-off lines: a shale cut-off line at a maximum gamma ray reading; and a sand cut-off line at the minimum gamma ray reading. High reading of gamma ray near

the shale line represented shale layers, while low gamma ray readings near the sand line represented non-shale layers. Once the overburden gradient and the shale intervals were identified for each well, the pore pressure and fracture pressure models could be estimated using three methods: Eaton's resistivity method; Eaton's sonic method; and Bower's interval velocity method.

2.3.3 Salt Diffusion

Salt diffusion is a process that allows ions or molecules to move from where they are more concentrated to where they are less concentrated. In rare cases, the salinity of water immediately below a salt seal can be significantly higher than proceeding depths due to salt diffusion. This observation was made for several offset wells and must be taken into account. Since Resistivity logs measure the electrical resistivity of formations, a large increase in salinity will cause Resistivity readings to decrease. This decrease can create erroneous pore pressure and fracture pressure predictions. It is important to have an accurate Sonic log measurements for pore pressure modeling because they are not affected by salinity.

Figure 1 below illustrates an example of salt diffusion. A four-track "quad combo" is displayed: a green gamma ray log; a red resistivity log; a pink bulk density log; and a blue sonic log. The fifth track places the sonic and resistivity logs together to show the effects of salt diffusion, represented as a neon green color. As observed, immediately below the salt, the resistivity is showing decreased readings while the sonic log is unaffected by the salt diffusion. At larger depths, the resistivity log and the sonic

log begin to share similar measurements. The resistivity log is no longer affected by salt diffusion at these depths.

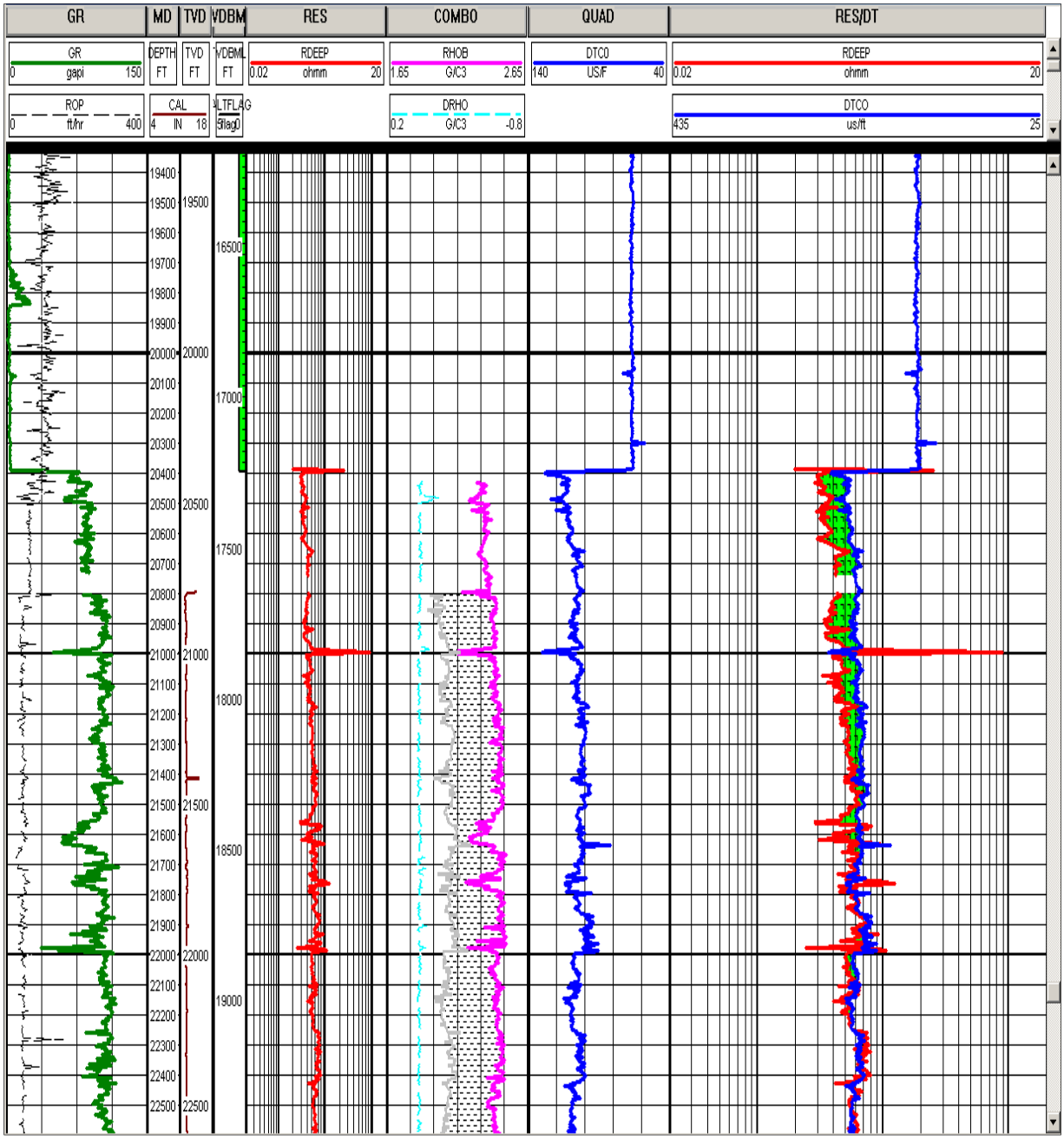

Figure 1. Example of salt diffusion.

2.3.4 Eaton's Resistivity Method

An assumption is made that the salinity of water is constant throughout the formation. Changes in salinity, and thus in the resistivity log, suggest a change in the shale porosity. Eaton's resistivity method uses the differences in resistivity and the normal compaction trend to find the pore pressure.

$$PP = OBG - (OBG - PPn)(Rob / Rnml)x \quad (3)$$

Where,

PP = Pore pressure gradient, ppg

OBG = Overburden gradient, ppg

PPn = Normal pore pressure gradient, 8.7 ppg

Rob = Observed shale resistivity, ohm-m

Rnml = Normal compaction trend shale resistivity, ohm-m

x = Empirical exponent, 1.2

2.3.5 Eaton's Sonic Method

Sonic measurements, or travel times, of normal compacted sediments decreases with depth due to decrease in porosity. Similar to Eaton's resistivity method, a normal compaction trend is applied to the sonic measurements. Travel times that decrease less than the normal compaction trend suggest an overpressure due to pore fluids being unable to escape as rapidly as necessary. Eaton's sonic method uses the difference in travel times and compaction trend to calculate the pore pressure.

$$PP = OBG - (OBG - PP_n)*(S_{ob} / S_{nml})^x \quad (4)$$

Where,

OBG = Overburden gradient, ppg

PPn = Normal pore pressure gradient, 8.7 ppg

Sob = Observed shale sonic transit time, μ/ft

Snml = Normal compaction shale sonic transit time, μ/ft

x = Empirical exponent, 3

2.3.6 Bower's Interval Velocity Method

Similar to Eaton's method, Bower's method uses a compaction trendline and finds the difference in measurements to estimate the pore pressure. However, Bower observed that some abnormal pressures beginning at or near the mudline in deep water showed curved normal compaction trend. This was the case with seismic interval velocity data for offset and prospect wells.

$$PP = S_v - [(V - V_{mudline})/a]^{1/b} \quad (5)$$

Where,

Sv = Overburden vertical total stress, psi

V = Velocity at given depth, ft/s

Vmudline = Seismic interval velocity at mudline, 5000 ft/s

a,b = Compaction trend coefficients

Seismic data can have significant changes with depth. To create an efficient pore pressure model, seismic interval velocity is smoothed towards shale responses. In these wells at depths above 10,000 - 15,000 feet, higher velocity readings represent shales. However, at a certain depth seismic responses in shale zones becomes the same or slower than in sands. Below 25,000 feet, shale zones are represented by the lower seismic interval velocity measurements.

2.3.7 Drilling Data

Drilling data from the offset wells is an important addition to pore pressure and fracture pressure study. In each study, four types of physical drilling data was used:

- MDT: Modular Dynamic Formation Test
- LOT: Leak-Off-Test
- MW: Mud weight
- CSG: Casing design

MDT, also known as Modular Dynamic Formation Test, is a wireline tool that takes real-time formation pressure measurements. It can also be used to take fluid samples and measure permeability. In the model, MDT pressure points act as physical pore pressure data points. Accurate pressure and permeability measurements result from high-resolution gauges combined with precise flowline control.

LOT, or leak-off-test, determines the strength or fracture pressure of the open formation. This test is conducted immediately after drilling below a new casing shoe.

During this test, the well is shut in and fluid is pumped into the wellbore to gradually increase the pressure that the formation experiences. At some pressure, fluid will enter the formation, or leak off. The result is the maximum pressure the formation can handle, also known as fracture pressure.

The mud weight and casing design used to drill offset wells is easily accessible data and can be found for almost any well. Well reports provide mud weights at each casing point and describe any problems encountered during the drilling process. The mud log records mud weights at shorter depth intervals and therefore can add the benefit of a more accurate mud weight profile.

2.3.8 Pore Pressure Calibration and Fracture Pressure

Once the respective models are created, they can be calibrated respectively using drilling data such as MDTs, LOTs, and Mud Weights. Drilling data of offset wells is manually imputed into the program from drilling reports. The empirical constants of the normal compaction trends, “a” and “b”, are user-defined constants that can be appropriately changed to calibrate the pore pressure models and fitted to physical drilling data. Fracture pressure models are constructed once the final calibration of pore pressure models concludes.

$$(shmin - pp) / (sv - pp) = km \quad (6)$$

Where,

Shmin = Minimum horizontal stress

Sv = Overburden stress

Pp = Pore pressure

Km = Matrix stress coefficient

The empirical normal compaction trend values “a” and “b” can later be applied to prospect wells to create pre-drill and real-time pore pressure and fracture pressure models. Pre-drill evaluation of prospect wells is done using Bower’s seismic interval velocity method. Only interval seismic velocity data is available for prospect wells. Once drilling begins on a project, Eaton’s resistivity and Eaton’s sonic methods are used to monitor and necessarily alter pore pressure and fracture pressure models in real-time as the drilling occurs.

CHAPTER 3: RESULTS

More than thirty offset wells were initially analyzed for the pore pressure and fracture pressure study of Prospect A and Prospect B. Five offset well models were created for Prospect A and two offset well models were created for Prospect B. As described in the previous chapters, the following steps were taken to perform pore pressure and fracture pressure analysis on the two prospects:

1. Find most suitable offset wells for Prospect A and Prospect B
2. Quality control data
3. Create overburden gradient using bulk density log
4. Identify shale zones using gamma ray log
5. Using the shale points for deep resistivity log, sonic log, and seismic interval velocity, create normal compaction trend for each method
6. Estimate pore pressure and fracture pressure for offset wells using Eaton's resistivity and sonic methods
7. Calibrate models using drilling data and compare to original offset data
8. Create synthetic bulk density curve for Prospect A and Prospect B using offset wells bulk density for each respective prospect well
9. Estimate pore pressure and fracture pressure for prospect wells using Bower's seismic interval velocity method
10. Calibrate models using offset data
11. Create safest and most efficient casing design

In this chapter, the results will be analyzed and discussed in greater detail. Table 3 and Table 4 show results of normal compaction trend empirical constants of offset wells for Prospect A and Prospect B, respectively. The final Bower's seismic interval velocity models were applied to each prospect. Table 5 displays the results of empirical constants for Prospect A and Prospect B.

Table 3: Prospect A offset wells' parameters for three methods

	Eaton's Resistivity			Eaton's Sonic			Bower's Seismic Interval Velocity	
	x	A	B	x	A	B	A	B
Well A1	1.2	0.01	0.000037	3	2.05	0.00002	14.2	0.714
Well A2	1.2	-0.37	0.000062	3	2.012	0.000015	14.2	0.753
Well A3	1.2	-0.06	0.00004	3	2.05	0.00002	14	0.735
Well A4	1.2	0.08	0.00003	3	2.12	0.000034	14.2	0.73
Well A5	1.2	0.08	0.000035	3	2.13	0.000034	14.2	0.754

Table 4: Prospect B offset wells' parameters for three methods

	Eaton's Resistivity			Eaton's Sonic			Bower's Seismic Interval Velocity	
	x	A	B	x	A	B	A	B
Well B1	1.2	-0.5	0.000085	3	2.05	0.000025	15	0.8
Well B2	1.2	-0.15	0.00004	3	2.05	0.000015	14	0.67

Table 5: Empirical constants for Prospect A and Prospect B

	Bower's Seismic Interval Velocity	
	A	B
Prospect A	14.15	0.75
Prospect B	14.5	0.8

3.1 Prospect A Offset Wells

The table below describes four different parameters of offset wells used in the pore pressure and fracture pressure study for Prospect A: water depth; measured depth of well; true vertical depth of well; and location of salt seal. The water depth of offset wells for Prospect A varies from 2,800 ft to 5,000 ft. Each well is fairly deep, with depths reaching as deep as 32,000 ft. Small differences in measured depths and true vertical depths suggest that the offset wells are vertical. Although Well A4 does not reach the salt seal, it is a great model to use in the analysis of Prospect A because of the similarities they share. Seismic maps suggest that Well A4 and Well A5 resemble the most analogous wells in terms of structure of the formation. They are, in fact, the closest wells to Prospect A with respect to location. Well A4 and Well A5 were the most appropriate wells to use in modeling pore pressure and fracture pressure of Prospect A; however, neither well was sufficient enough to model pressures far away from the salt seal due to smaller well depths. This issue was resolved using Well A1, A2, and A3. These wells were deep enough to help create an accurate Prospect A model for deeper depths.

Table 6: Description of Prospect A offset wells

	Water Depth	MD	TVD	Salt Seal
	ft	ft	ft	ft
Well A1	4908	29749	29680	8855 - 14039
Well A2	4334	31131	29062	9724 - 21919
Well A3	4986	31146	29697	9205 - 13121
Well A4	2828	22580	22576	22000 - 23000
Well A5	2920	26569	26552	21190 - 22150

3.1.1 Offset Well A1

Figure 2 through Figure 5 below show the results from steps taken to create pore pressure and fracture pressure models for Well A1. Shale points for resistivity, sonic, and seismic interval velocity are picked out using the gamma ray log. If the curve is too sensitive, a smoothing application can be used to make the curve smoother. Sharp changes in measurements of log data can greatly affect the resulting pore pressure and fracture pressure models. Once the non-shale points are excluded, a normal compaction trend is placed on each curve. The normal compaction trend coefficients can be altered to calibrate the pore pressure to the MDT pressure points and mud weight curve obtained from drilling data. The final calibrated pore pressure and fracture pressure model for Well A1 using Eaton's resistivity and sonic methods is displayed below. As Figure 3 suggests, both method agree with MDT pressure points and mud weight gradient. LOT pressure points line up fairly well on the fracture pressure curve.

The salt seal of Well A1 is located at a depth range of 8,855 to 14,039 ft. It is the shallowest salt seal out of all the offset wells. The pore pressure and fracture pressure above 14,039 ft are ignored because of unreliable data. Accurate Resistivity log and Sonic log readings begin at 18,000 ft. Data above this depth was synthetically generated using the gamma ray log to provide a consistency in log readings. The pore pressure and fracture pressure models between 20,000 ft and 30,000 ft closely follow the mud weight curve. Eaton's resistivity and sonic methods show a huge increase in pore pressure below the salt. At a depth of 14,100 ft, the pore pressure gradient is 12.5 ppg and the fracture pressure gradient is 14. At the bottom of the well at a depth of 30,000 ft, the pore

pressure gradient is 15 ppg and the fracture pressure gradient is 16.75 ppg, giving us a 1.75 ppg window.

Three types of velocities were available for each offset well; however, only seismic interval velocity was used. The other seismic curves showed little to no variation in data with depth and would be impossible to use as a tool for pore pressure estimation. Similar to Eaton's resistivity and sonic methods, the seismic interval velocity curve may be smoothed to create a more efficient pore pressure and fracture pressure model. Shallow depths of seismic interval velocity are ignored due to inconsistencies in data. Figure 5 illustrates the resulting pore pressure and fracture pressure models using Bower's seismic interval velocity method. The seismic interval velocity pore pressure curve agrees with MDT pressure points and mud weight data, and the fracture pressure aligns with LOT pressure points. The three pore pressure and fracture pressure methods used for Well A1 correlate with measured drilling data. The results show that at depths below the salt seal the mud weight window ranges between 1.5 to 3 ppg.

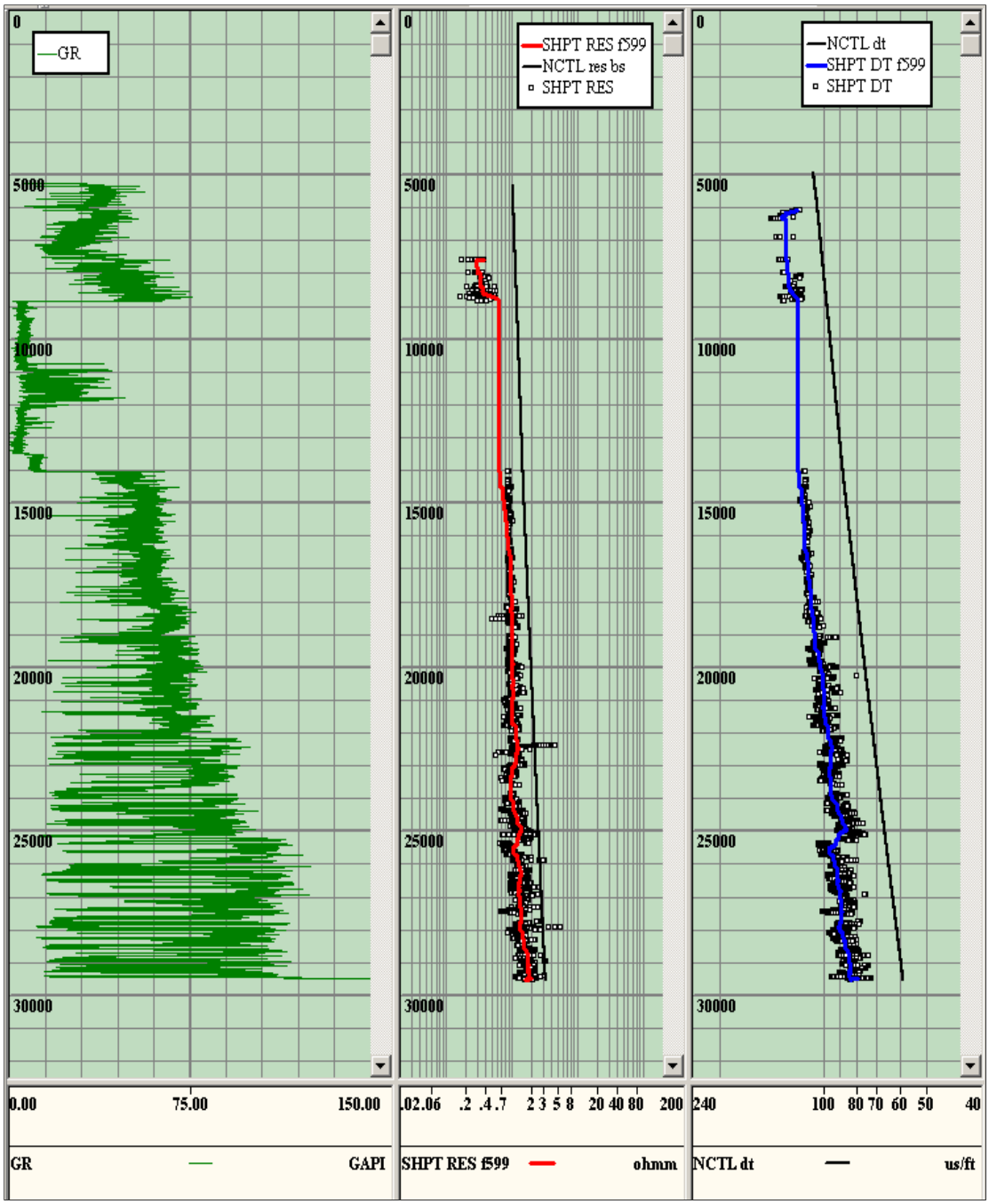

Figure 2. Shale point intervals and normal compaction trend of Eaton's resistivity and Eaton's sonic method for Well A1

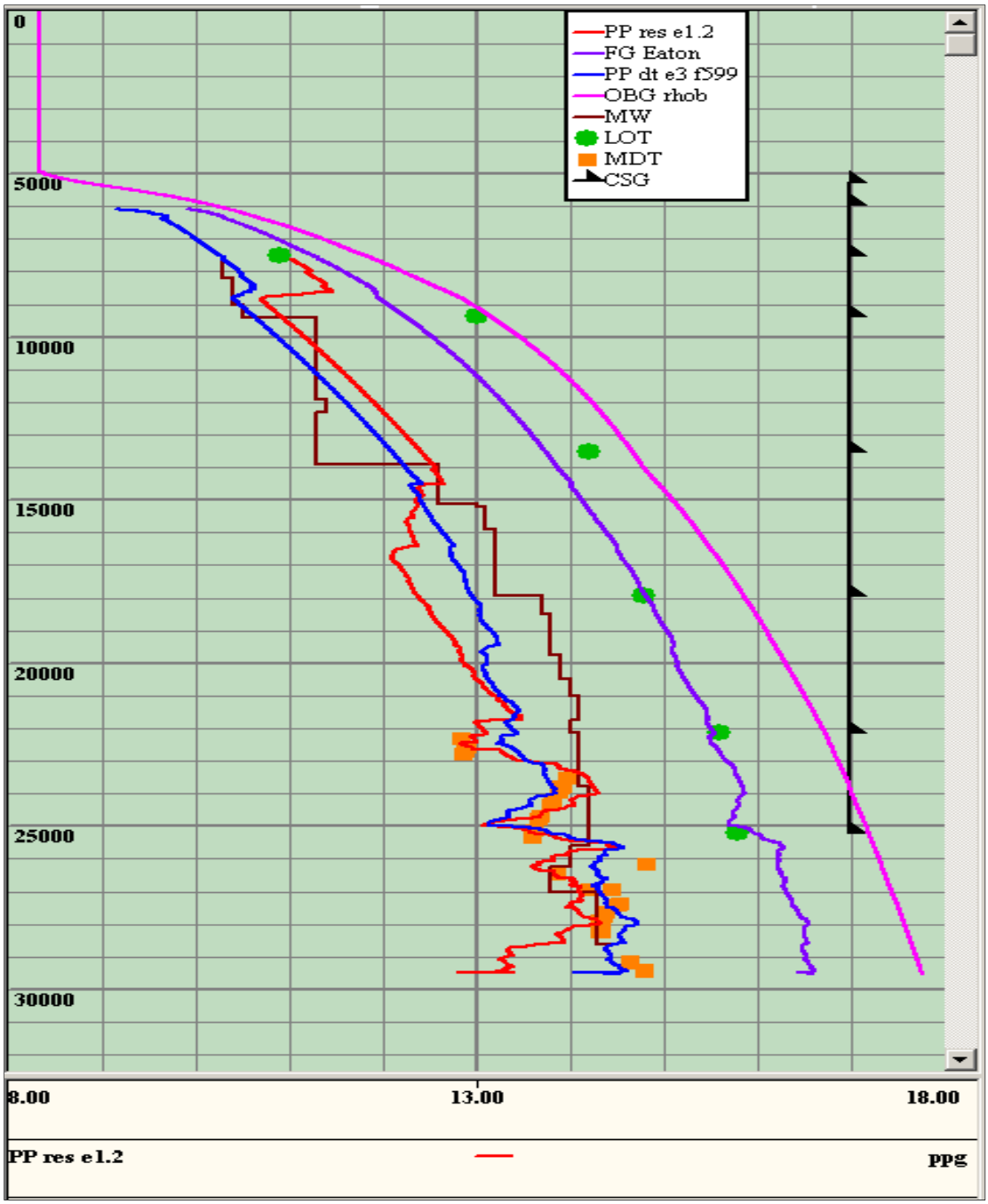

Figure 3. Calibrated pore pressure and fracture pressure models of Eaton's resistivity and Eaton's sonic method for Well A1

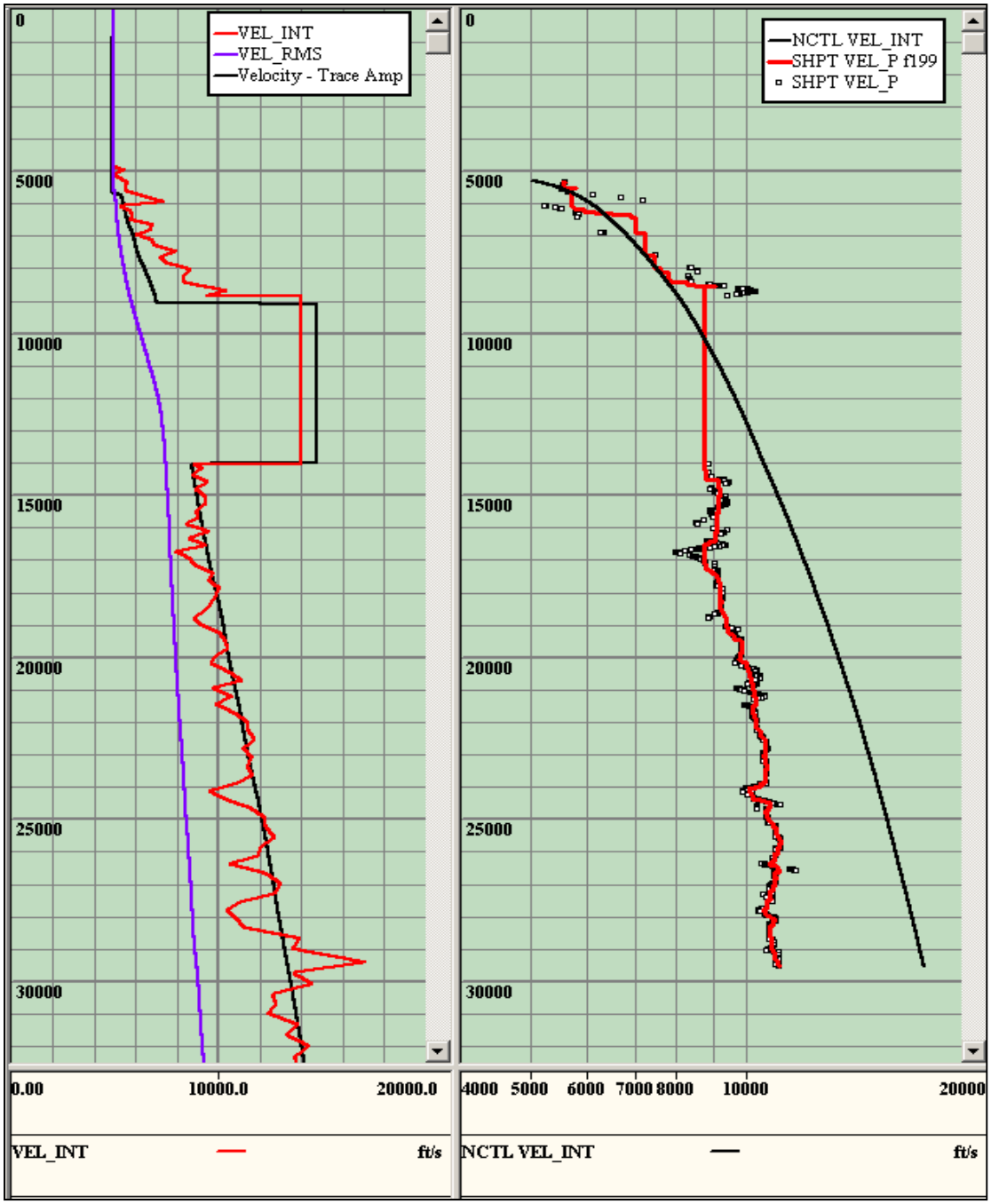

Figure 4. Seismic interval velocity and normal compaction trend of Bower's method for Well A1

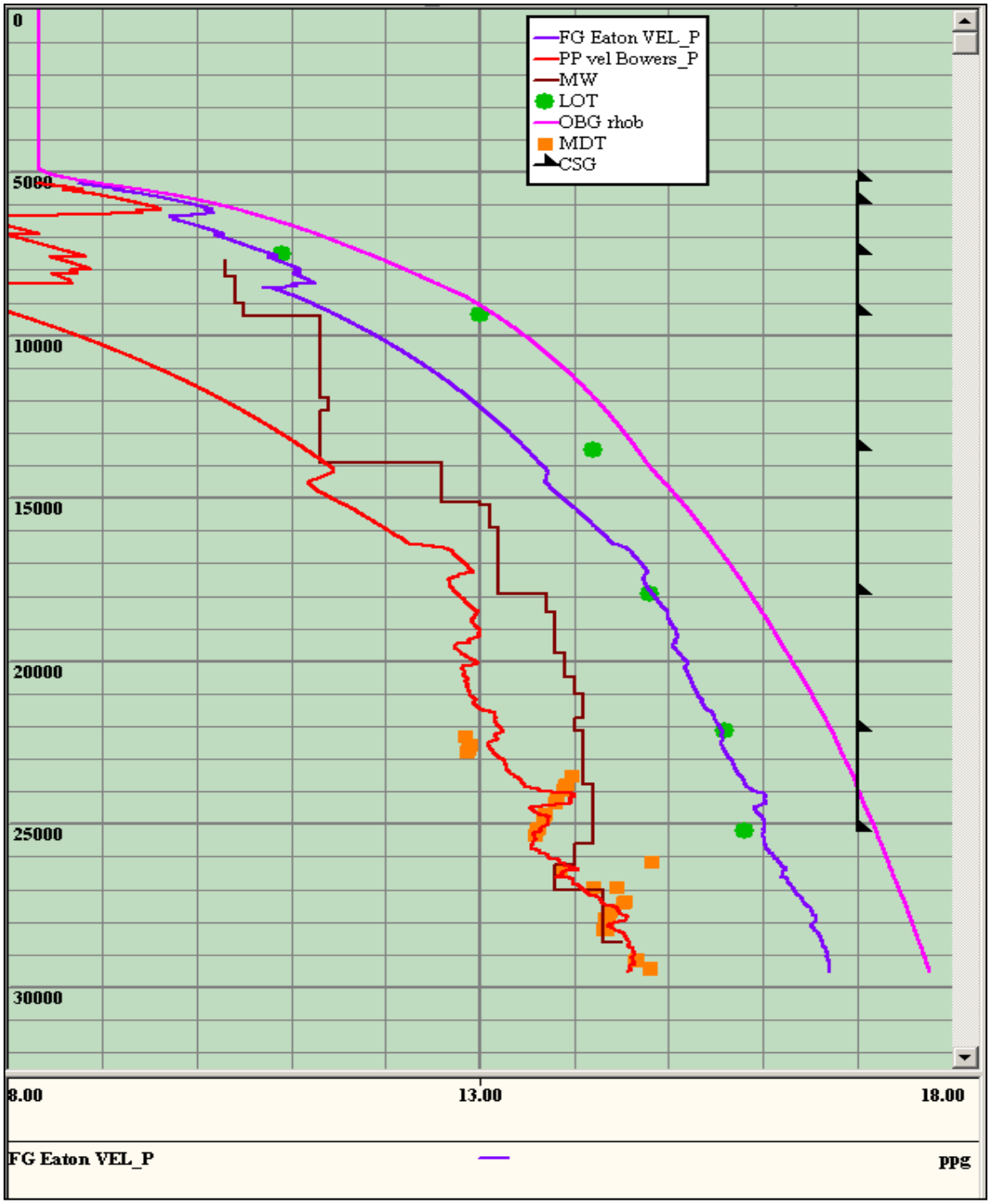

Figure 5. Calibrated pore pressure and fracture pressure model of Bower's seismic interval velocity method for Well A1

3.1.2 Offset Well A2

The results for Well A2 pore pressure and fracture pressure models using Eaton's resistivity, Eaton's sonic, and Bower's seismic interval velocity methods are displayed in Figure 6 through Figure 9. The results are not as reliable as in Well A1. The salt seal in Well A2 is located at a depth range of 9,724 to 21,919 ft. All data above 22,000 ft is ignored due to unreliability. Resistivity readings below the salt may rarely display a bowl shaped pattern, first decreasing then slowly increasing; this is due to salt diffusion. These incorrect measurements can create problems with pore pressure and fracture pressure models and must be ignored or altered manually. Sonic LWD readings ranged from 24,000 to 30,000 ft. A synthetic curve generator was run for the rest of the depths, which created a curve that follows the same pattern as the resistivity log. Pore pressure and fracture pressure readings ranging from 21,000 ft to 24,500 ft are therefore also ignored. Sections of faulty pore pressure and fracture models can be easily noticed, as observed in Figure 7. At 22,500 ft, the pore pressure models increases significantly. This is due to the bowl-shaped decrease in Resistivity and Sonic logs below the salt.

Bower's method creates more accurate pore pressure and fracture pressure curves for deeper locations in the well. In this case, measurements at the salt and below the salt were ignored. MDT pressure points and LOT pressure points match up with the models starting at 21,000 ft. Right below the salt at 21,000 ft, the pore pressure and fracture pressure gradients are 13.25 and 15.25 ppg, respectively. At the bottom hole depth, the pore pressure gradient is 15 ppg and the fracture gradient is 16.25 ppg.

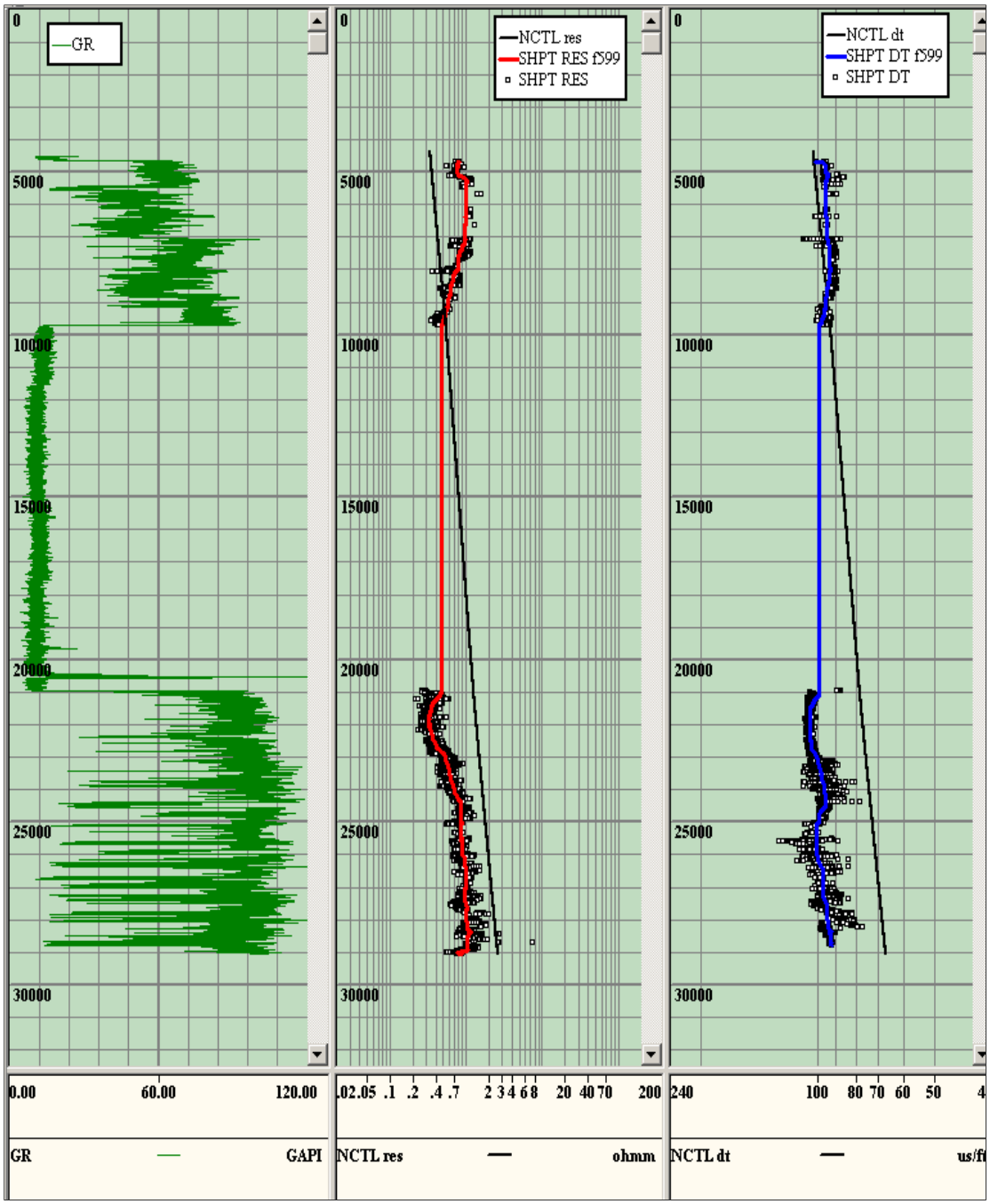

Figure 6. Shale point intervals and normal compaction trend of Eaton's resistivity and Eaton's sonic method for Well A2

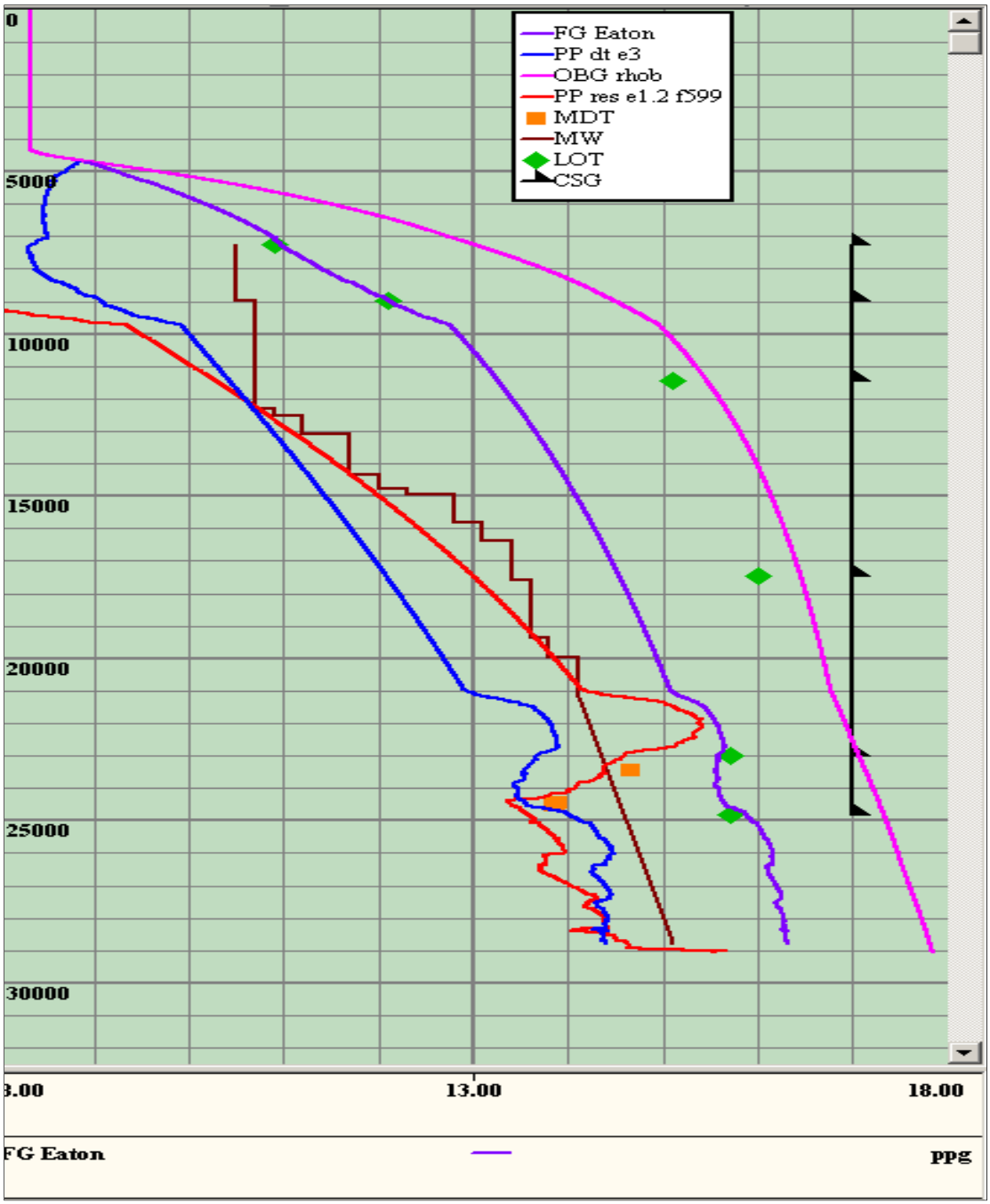

Figure 7. Calibrated pore pressure and fracture pressure models of Eaton's resistivity and Eaton's sonic method for Well A2

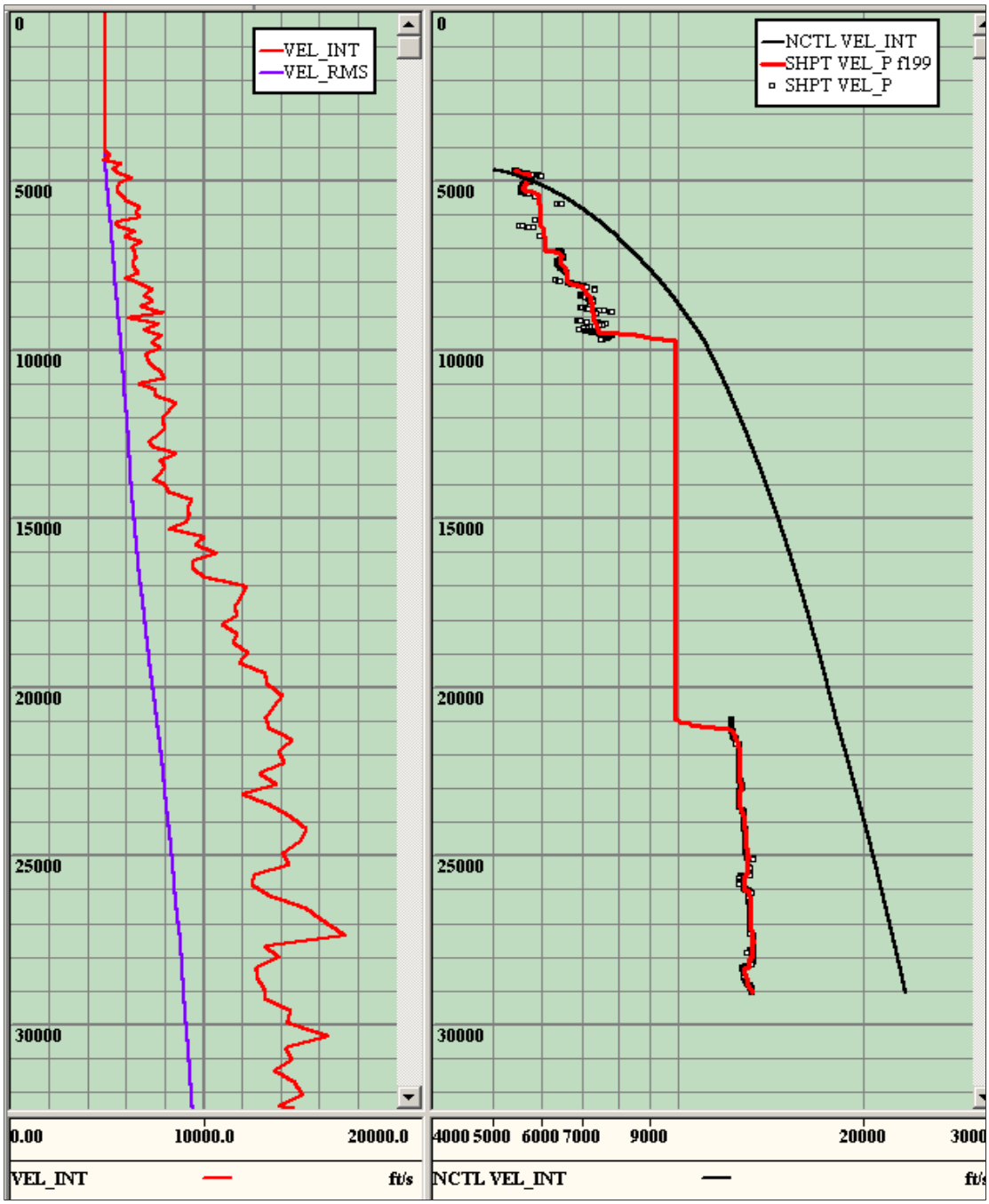

Figure 8. Seismic interval velocity and normal compaction trend of Bower's method for Well A2

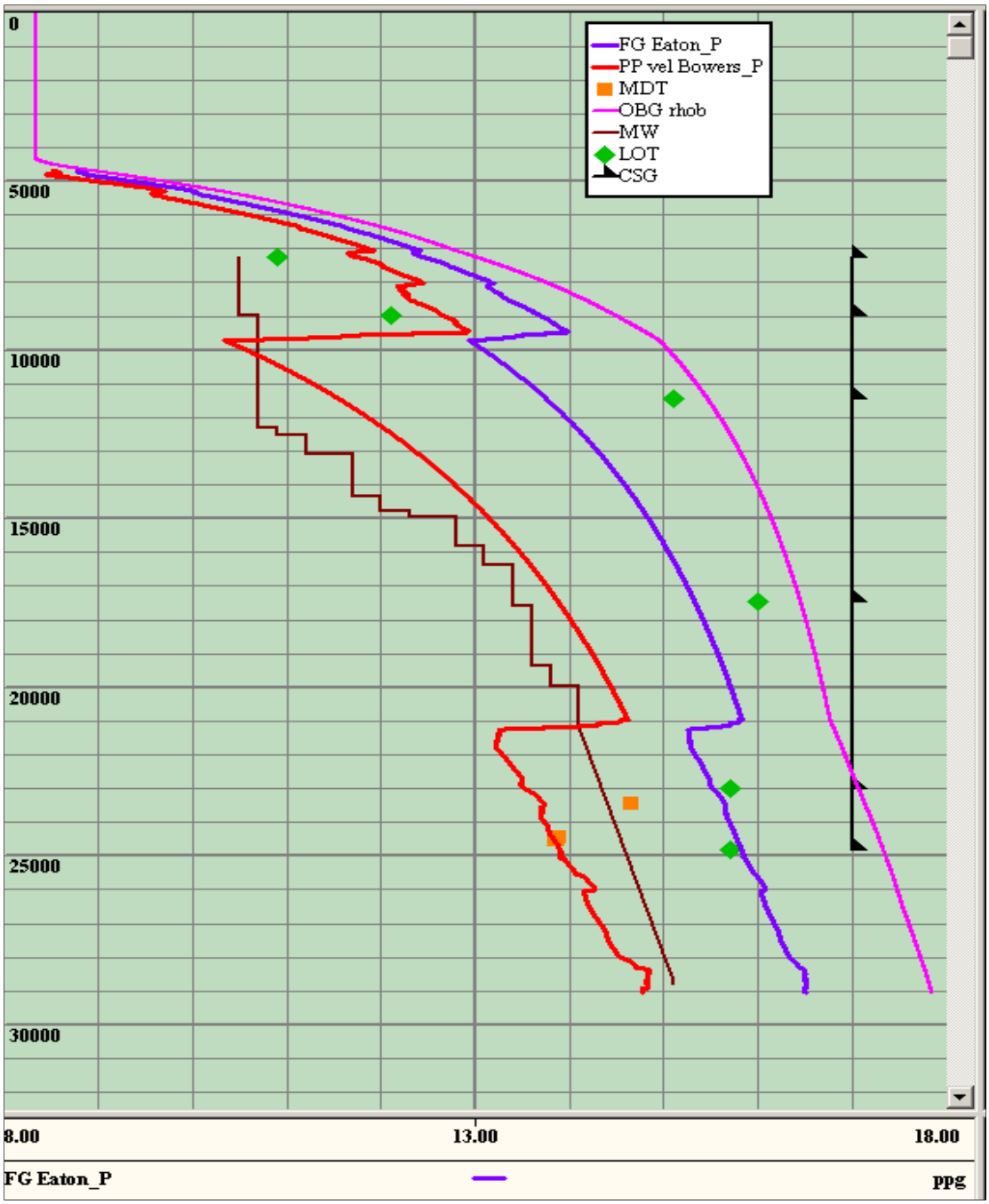

Figure 9. Calibrated pore pressure and fracture pressure model of Bower's seismic interval velocity method for Well A2

3.1.3 Offset Well A3

Well A3 is a near perfect offset well to use for pore pressure and fracture pressure modeling. High quality logs and drilling data are an important aspect for creating accurate estimations. A sharp increase in the resistivity immediately below the salt is observed. Again, this incorrect reading can be caused by improper tool measurements or salt diffusion. Salinity of the water in that section can be significantly higher, thus causing the resistivity measurements to increase. Therefore, pore pressure and fracture pressure models using Eaton's resistivity method must be carefully inspected below the salt seal. Necessary adjustments to the models can be made in real-time if this increasing resistivity trend is observed. On the other hand, sonic measurements are not affected by changes in salinity. Eaton's sonic method can provide accurate predictions of pore pressure and fracture pressure models around salt seals. This can be observed in Figure 11, which shows the resulting pore pressure and fracture pressure models using Eaton's resistivity and sonic methods.

Bower's method, illustrated in Figure 13, lacks the accuracy displayed by Eaton's methods. A large quantity of MDT pressure points and LOT pressure points benefits the creation and calibration of a precise mud weight window. MDT and LOT pressure points line up significantly well to Eaton's pore pressure and fracture pressure models. However, a less precise Bower's model is observed. The accuracy of the seismic interval velocity model may often relate to the extent of smoothing applied to initial data. Eaton's resistivity and sonic methods tend to always have more accurate pore pressure and fracture pressure models.

The salt seal in Well A3 ranges from 9,205 to 13,121 ft. Significant presence of salt in the well can defect the quality of logs and data, as observed in Well A2. Similar to previous offset wells, the average Mud Weight window below the salt is 1.5 to 2 ppg. Right below the salt at 13,200 ft, the pore pressure and fracture pressure gradients are 12.5 and 14 ppg, respectively. The pore pressure gradient at the bottom of the well, or 29,000 ft, is 14.7 ppg and the fracture pressure gradient is 16.5 ppg.

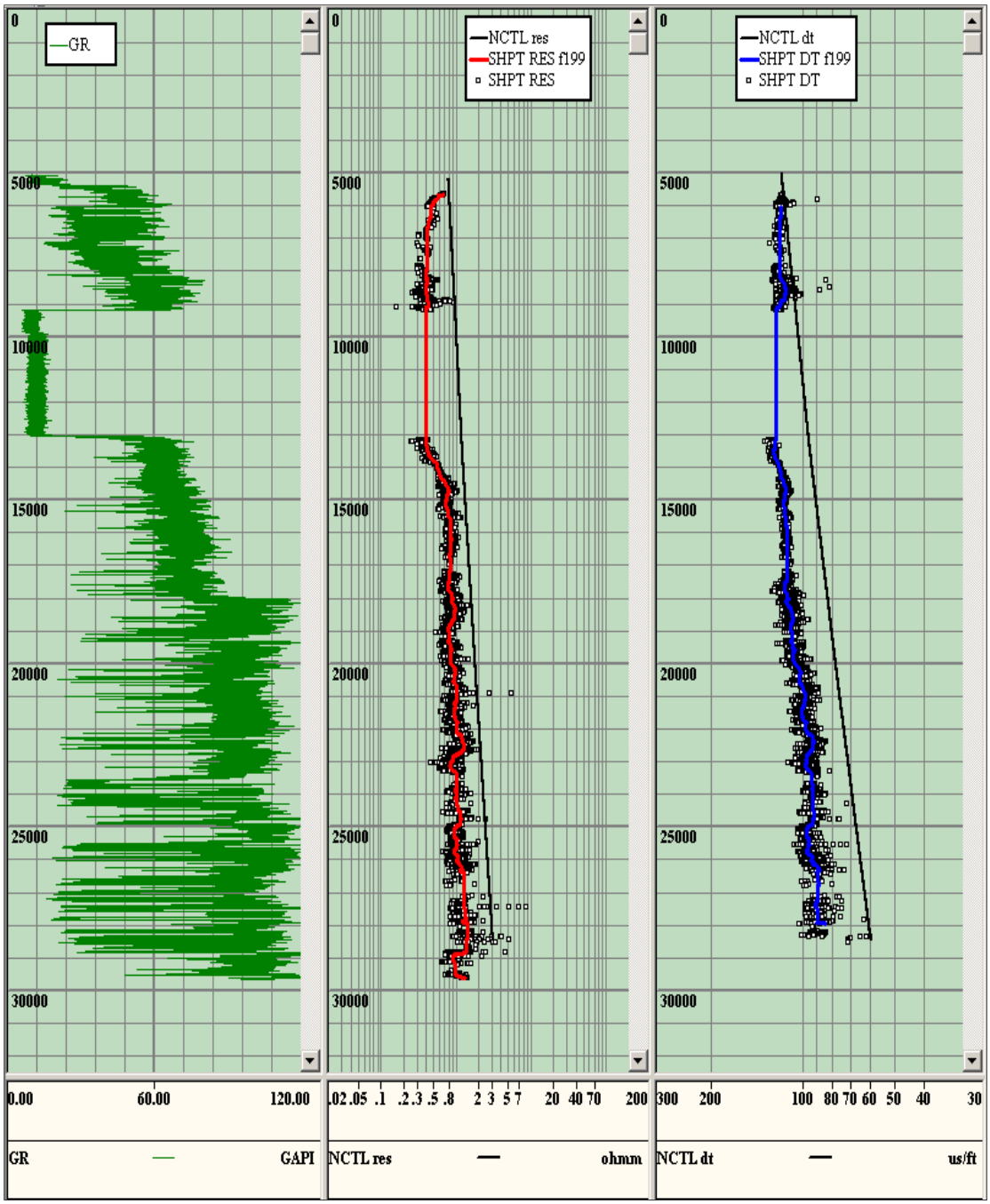

Figure 10. Shale point intervals and normal compaction trend of Eaton's resistivity and Eaton's sonic method for Well A3

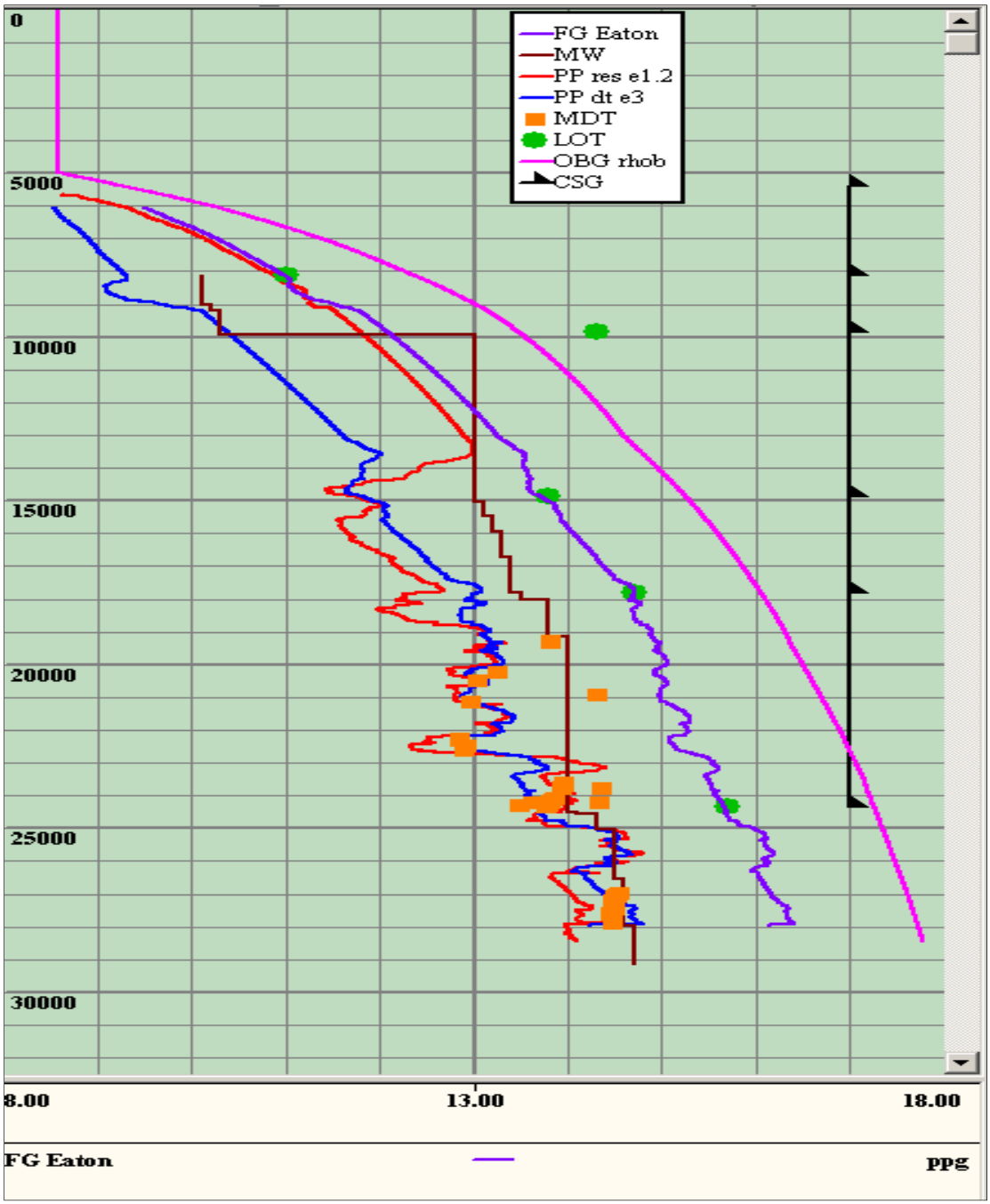

Figure 11. Calibrated pore pressure and fracture pressure models of Eaton's resistivity and Eaton's sonic method for Well A3

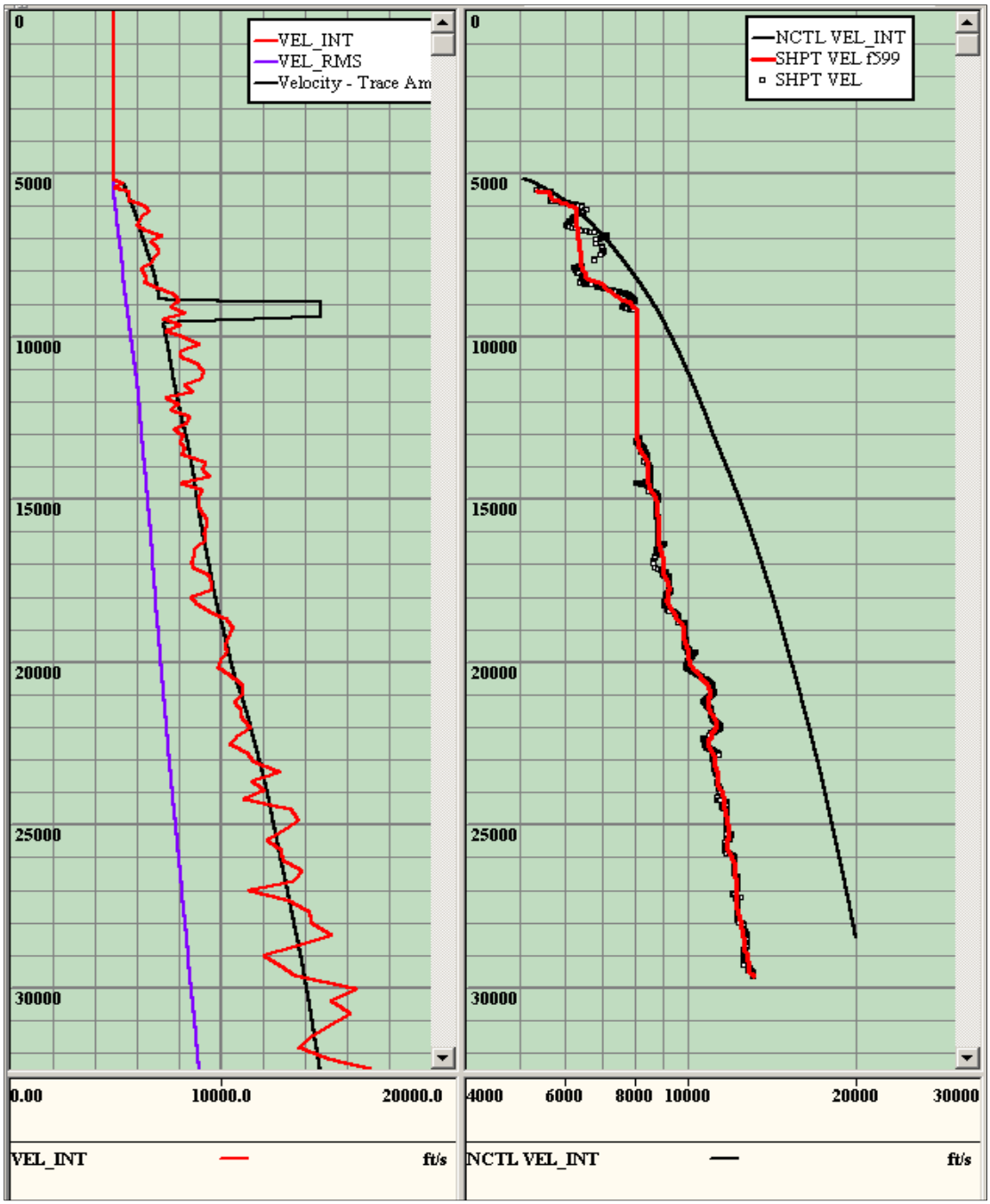

Figure 12. Seismic interval velocity and normal compaction trend of Bower's method for Well A3

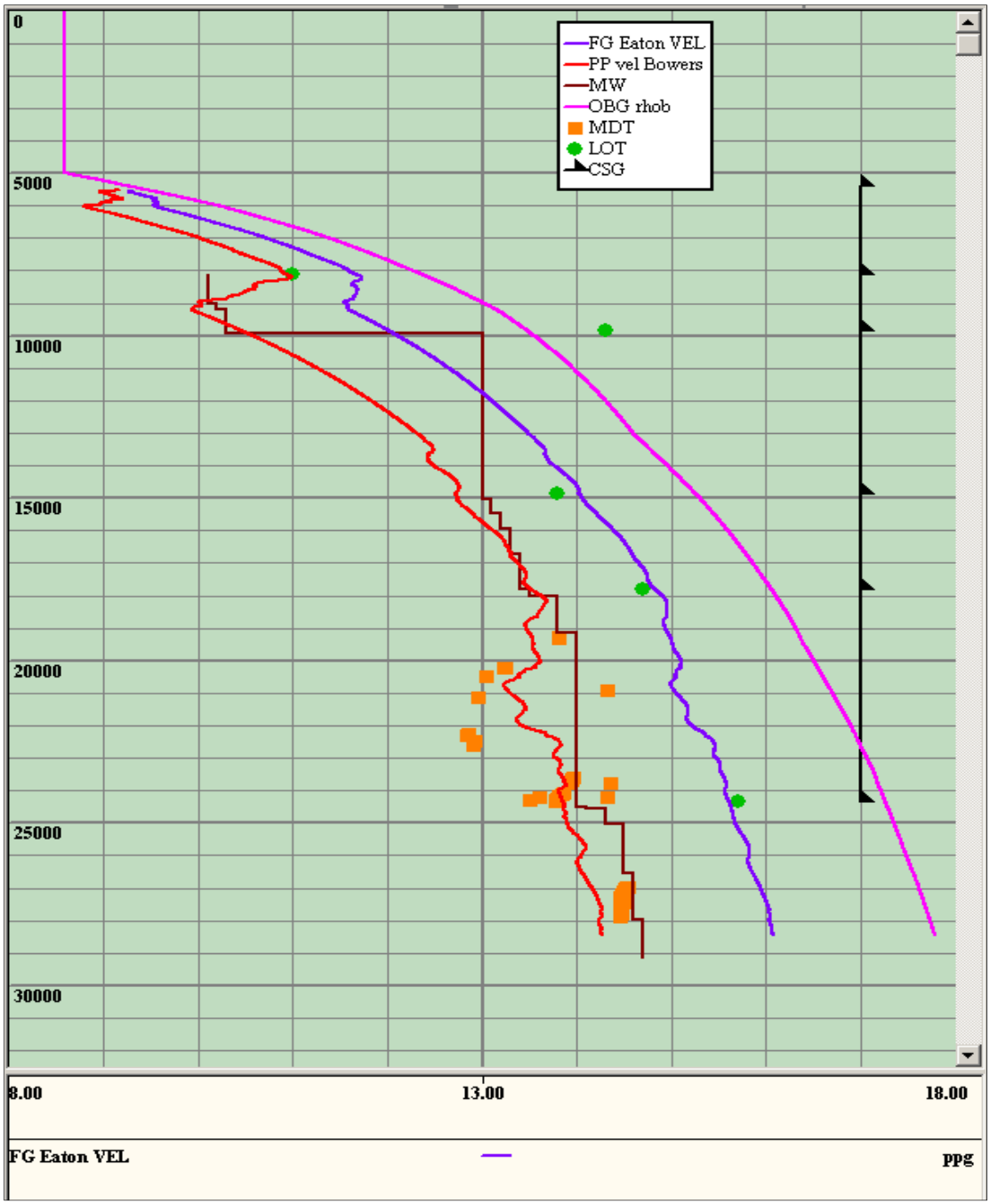

Figure 13. Calibrated pore pressure and fracture pressure model of Bower's seismic interval velocity method for Well A3

3.1.4 Offset Well A4

Well A4 provides a case where there is an abundance of drilling data but a lack of LWD log data. Although LWD log data is minimal, the quality of seismic interval velocity data is sufficient enough to create an accurate pore pressure and fracture pressure model, shown in Figure 17. LWD log readings fall several feet short of the salt seal. Resulting Eaton's resistivity and sonic models, presented in Figure 15, initially correlate with MDT pressure data and mud weight data. At 18,500 ft, the pore pressure models begin to deviate from the mud weight log. The quality of resistivity measurements are questioned due to the initial decrease and eventual increase in log readings. Resistivity of previous offset wells tend to show an increase with depth. An extreme increase or decrease in resistivity data will strongly affect the pore pressure model and create an inaccurate design. At 11,000 ft, Eaton's method shows a pore pressure gradient of 12.75 ppg and a fracture pressure gradient of 14.5 ppg.

Bulk density, displayed in Figure 16, was recreated using analogous bulk density data from offset wells using Equation 3.1. This method, described in greater detail in Chapter 3.3, was applied to the two prospect wells. On the same figure, seismic interval velocity and smoothed seismic interval velocity are displayed. As mentioned in the previous chapter, seismic interval velocity is smoothed towards shale responses. In this well at depths above 15,000 ft, higher velocity readings represent shales. Below 25,000 ft, shale zones are represented by the lower seismic interval velocity measurements.

Bower's pore pressure model for Well A4 correlates very well with MDT pressure points and mud weight drilling data. Seismic interval velocity readings stretch deeper

than LWD log data and reach the salt seal, located at 22,000 to 23,000 ft. Therefore, using seismic interval velocity to create pre-drill pore pressure and fracture pressure designs for the two deep prospect wells proves very beneficial. Bower's pore pressure and fracture pressure gradients for Well A4 at 30,000 ft are 16 ppg and 17.75 ppg, respectively.

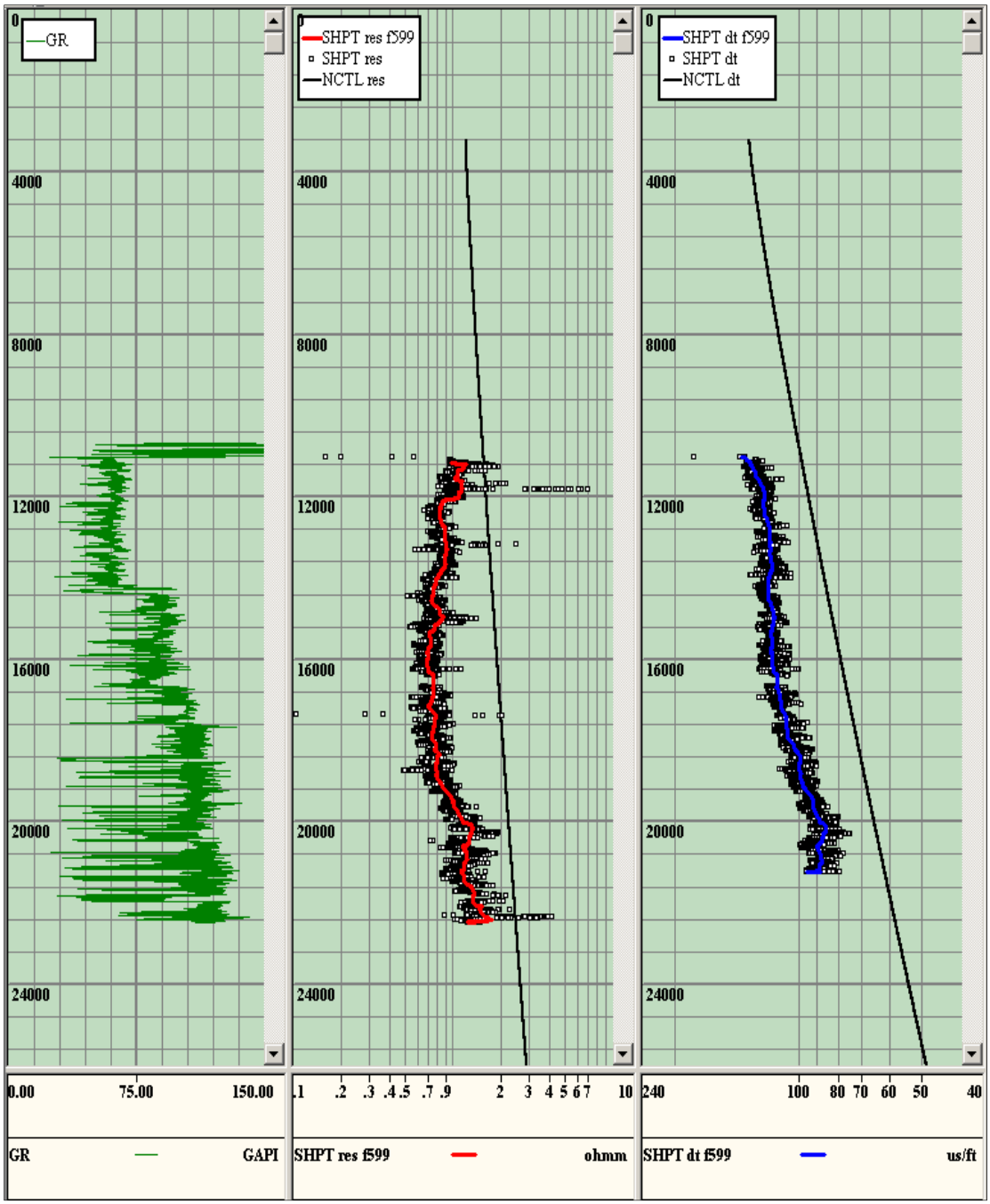

Figure 14. Shale point intervals and normal compaction trend of Eaton's resistivity and Eaton's sonic method for Well A4

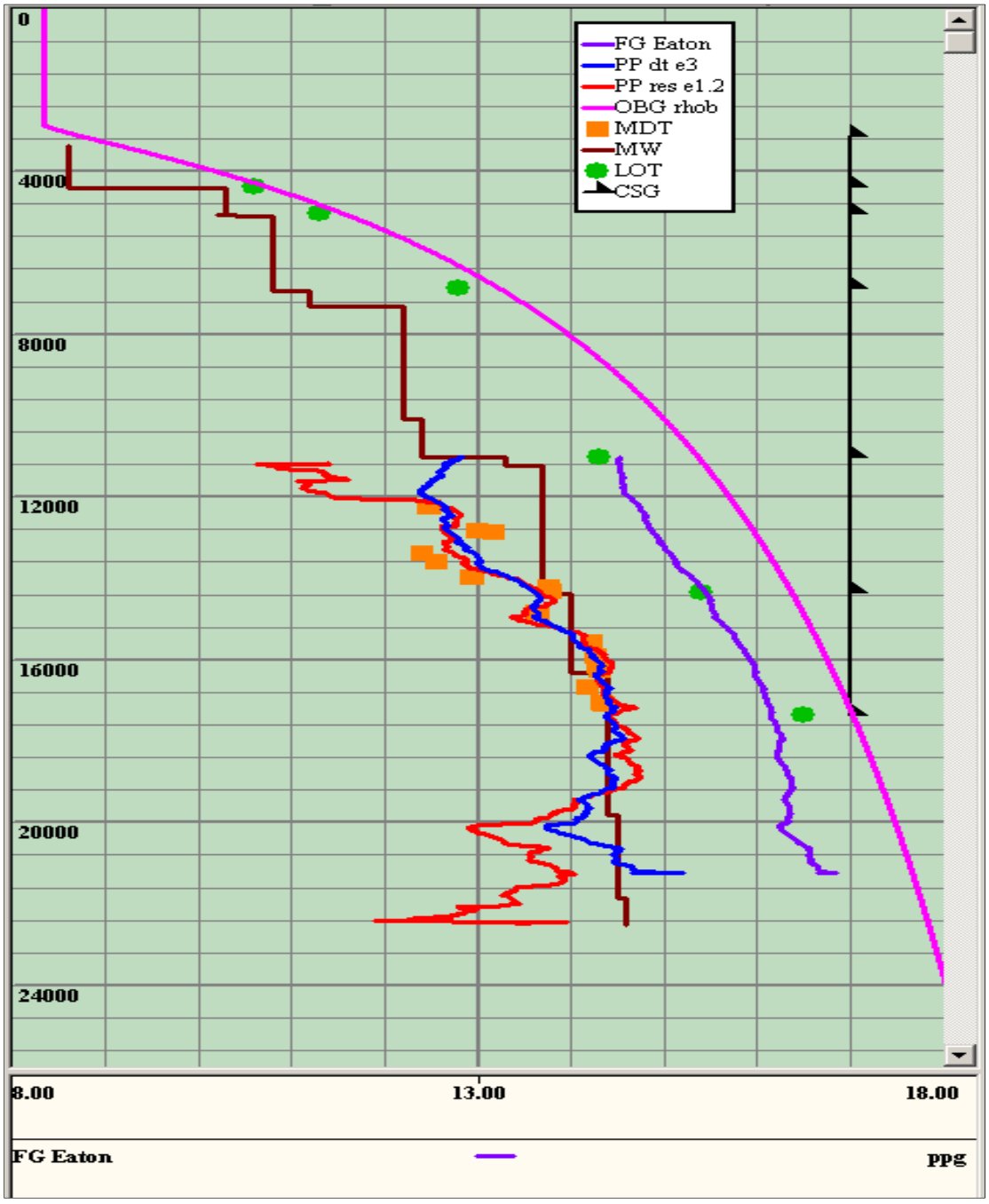

Figure 15. Calibrated pore pressure and fracture pressure models of Eaton's resistivity and Eaton's sonic method for Well A4

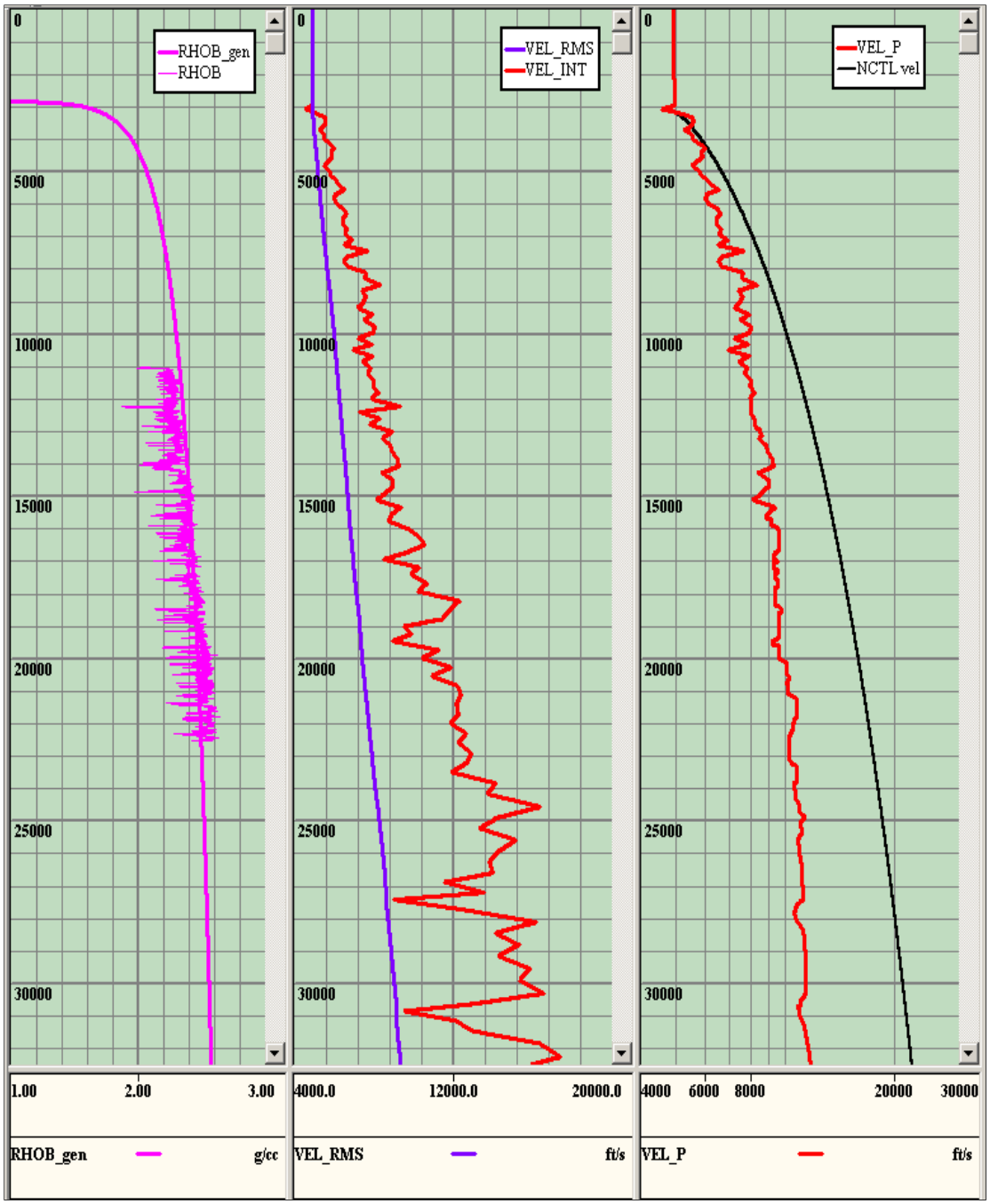

Figure 16. Generated bulk density, seismic interval velocity, and normal compaction trend of Bower's method for Well A4

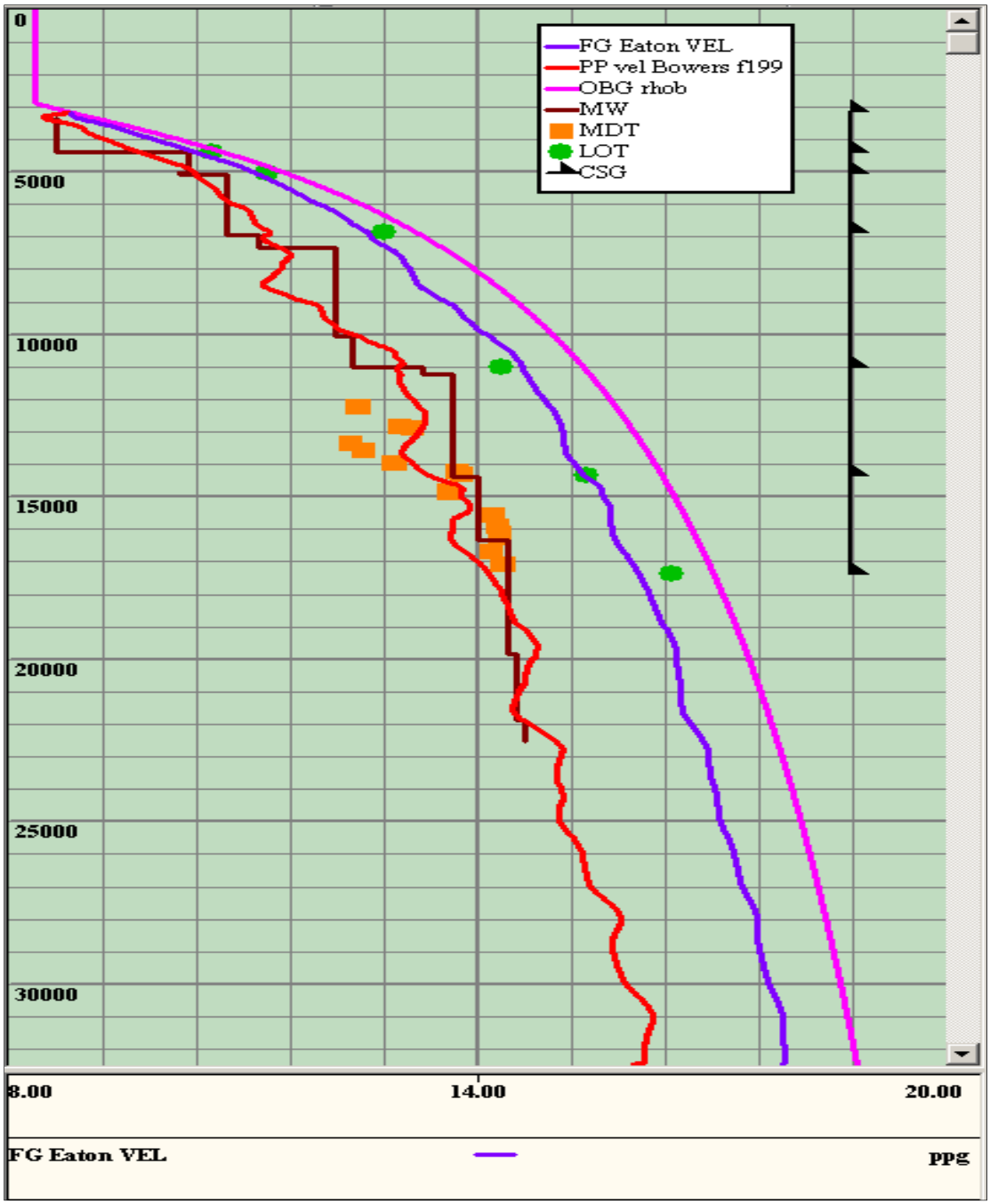

Figure 17. Calibrated pore pressure and fracture pressure model of Bower's seismic interval velocity method for Well A4

3.1.5 Offset Well A5

As stated above, Well A4 and Well A5 are the most appropriate wells to use in modeling a pre-drill pore pressure and fracture pressure design of Prospect A. Seismic maps suggest that Well A4 and Well A5 resemble the same formation structure as Prospect A. Similar to Well A4, Well A5 arguably lacks high-quality LWD log data, which it makes up with seismic interval velocity. However, Well A5 only has a limited amount of drilling data; MDT pressure points were taken at a depth range of 23,000 to 24,000 ft. Well A5 serves as a prime example of the importance of mud weight drilling data; pore pressure and fracture pressure was calibrated using only mud weight data, shown in Figure 19.

Drillers experienced problems with the wellbore at 21,000 ft. Casings were placed at 21,342 feet and 22,590 ft due to issues with pore pressure and the salt seal. This setback in drilling time can cause many financial problems. Figure 21 displays Bower's seismic interval velocity model. At 21,000 ft, pore pressure gradient is observed passing the mud weight drilling data curve. Problems arose at 21,000 ft, where mud weight was not high enough to support the pore pressure. Accurate pre-drill pore pressure and fracture pressure models would have prevented these setbacks.

The salt seal is located at a depth of 21,190 to 22,150 ft. Sonic data was only available below the salt, at a depth range of 22,000 to 26,500 ft. This data proved useful in creating a normal compaction trend to modeling pore pressure and fracture pressure. Both Eaton's resistivity and sonic pore pressure models followed the orientation of mud weight data and matched up to the limited MDT pressure points. The average mud weight

window below the salt ranged from 1 to 1.75 ppg. Right below the salt at 22,000 ft, the pore pressure and fracture pressure gradients are 14.5 and 16 ppg, respectively. The pore pressure gradient at the bottom of the well at, or 26,000 ft, is 15.85 ppg and the fracture pressure gradient is 17.75 ppg. Using Bower's model, at 30,000 ft the projected pore pressure gradient is 16.3 ppg and the fracture pressure gradient is 17.9 ppg.

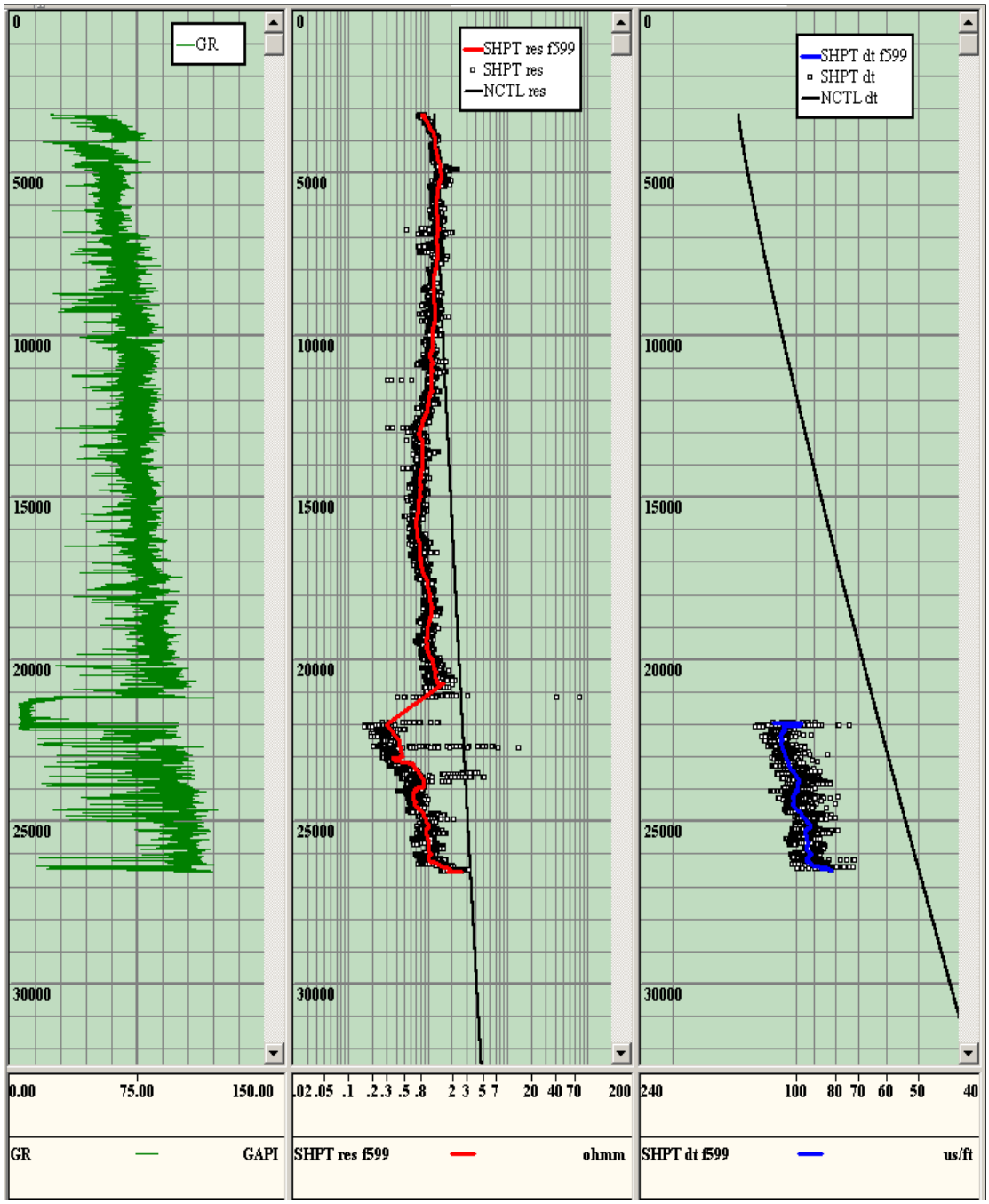

Figure 18. Shale point intervals and normal compaction trend of Eaton's resistivity and Eaton's sonic method for Well A5

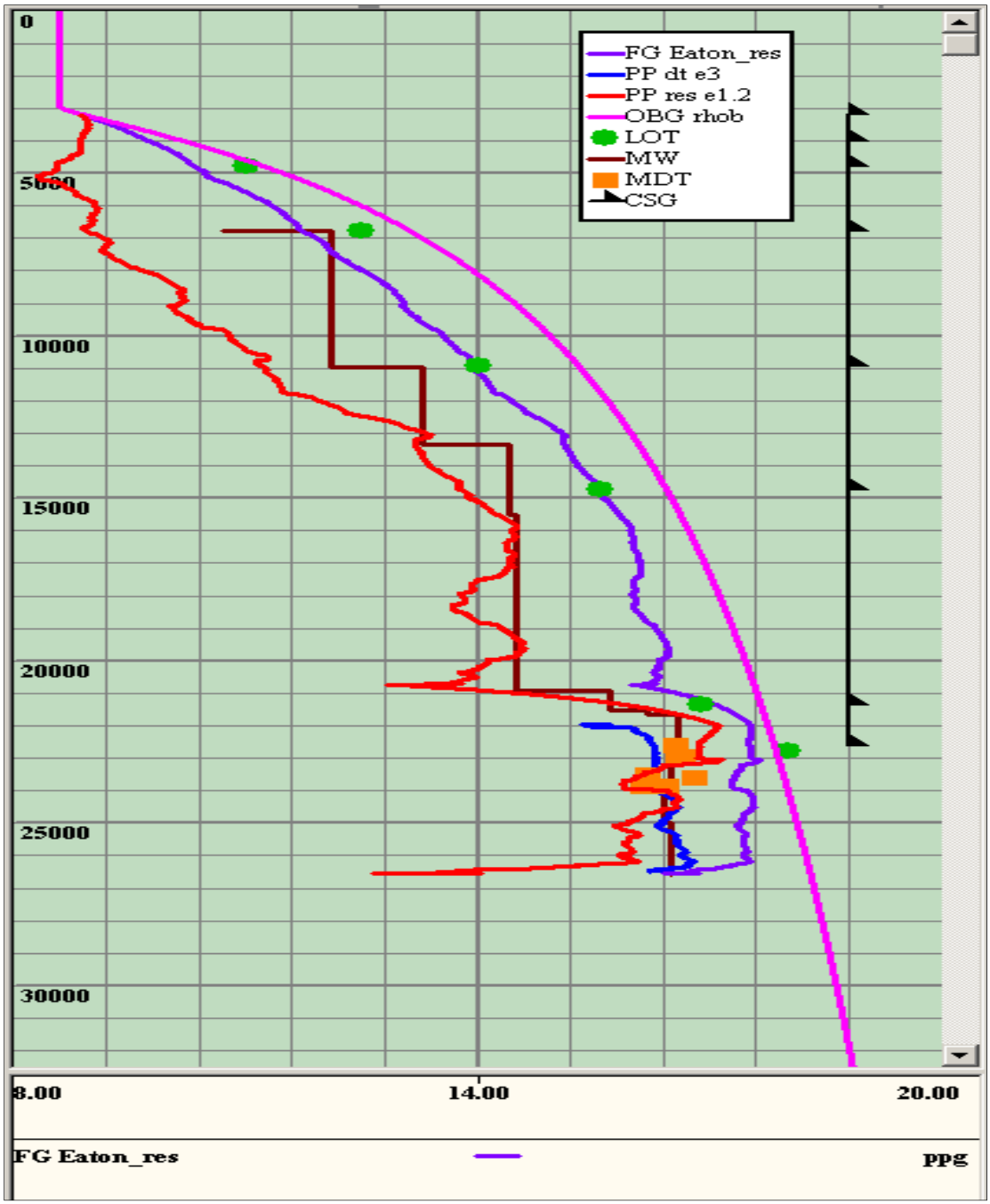

Figure 19. Calibrated pore pressure and fracture pressure models of Eaton's resistivity and Eaton's sonic method for Well A5

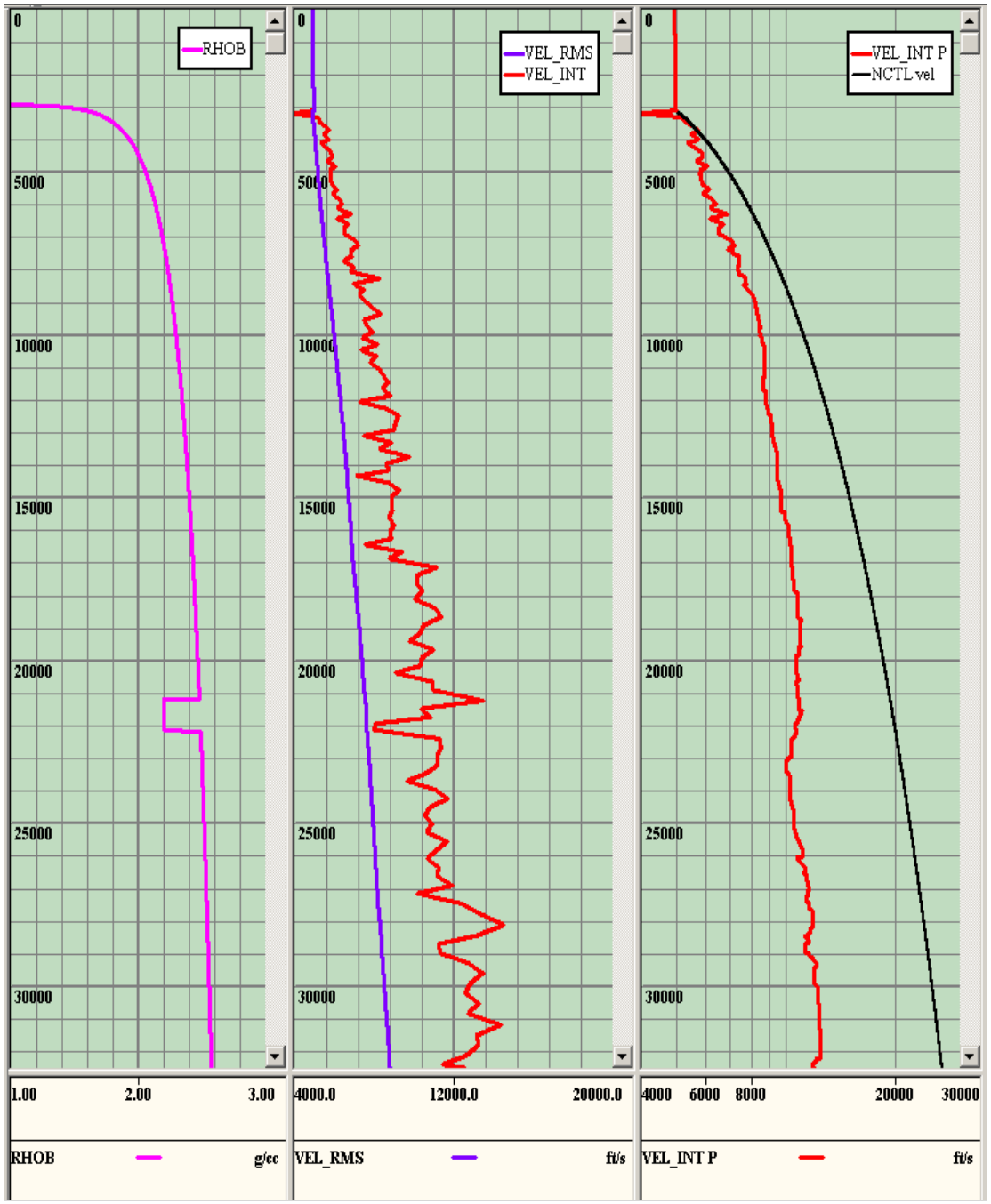

Figure 20. Generated bulk density, seismic interval velocity, and normal compaction trend of Bower's method for Well A5

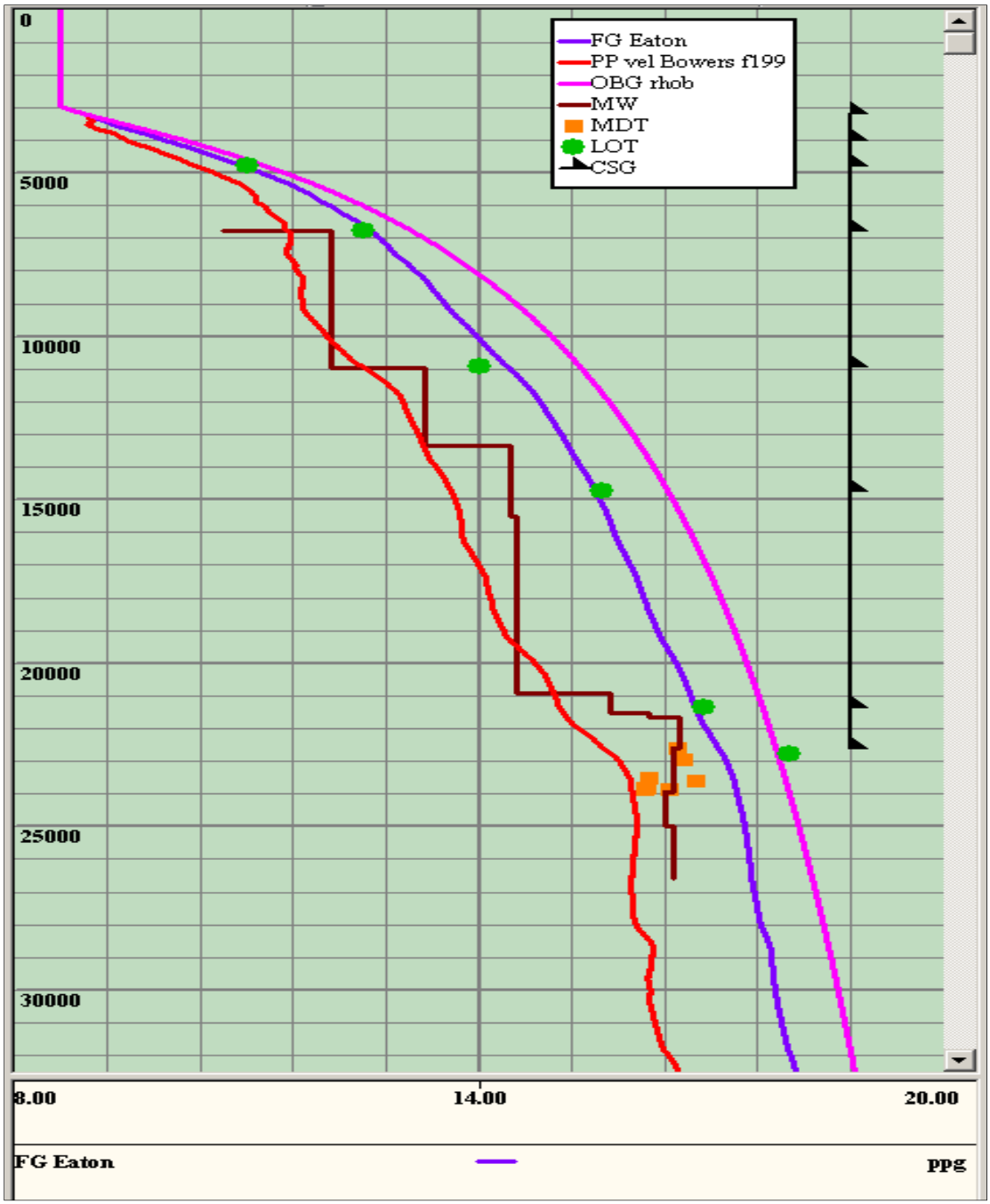

Figure 21. Calibrated pore pressure and fracture pressure model of Bower's seismic interval velocity method for Well A5

3.2 Prospect B Offset Wells

Contrary to the availability of Prospect A offset wells, only two offset wells were evaluated for the pore pressure and fracture pressure study of Prospect B. This was due to the location of Prospect B and the lack of wells with similar formation structures in the area. However, in the final pre-drill pore pressure and fracture pressure model, only Well B1 Bower's method was used. Well B2 seismic interval velocity data was too messy and created many problems in the pore pressure model. Table 7 below provides a description of the two Prospect B offset wells. Well B1 and B2 share similar water depths and bottom-hole depths. Both wells are fairly vertical and have a salt seal running to about 20,000 ft.

Table 7: Description of Prospect B offset wells

	Water Depth	MD	TVD	Salt Seal
	ft	ft	ft	ft
Well B1	4180	29894	29519	6647 - 19972
Well B2	4266	28736	28721	10994 - 19829

3.2.1 Offset Well B1

Well B1 was the first offset well to be used in the pore pressure and fracture pressure study of Prospect B. Figure 22 through Figure 25 display the steps and final models of pore pressure and fracture pressure using the three methods: Eaton's resistivity; Eaton's sonic; and Bower's seismic interval velocity. In this well, LWD data at and above the salt seal is either not available or ignored. A large quantity of MDT pressure points

were available to help calibrate the pore pressure and fracture pressure models, shown in Figure 23. However, at a depth range of 22,000 ft to 24,000 ft, MDT pressure points surpassed the mud weight used to drill the well. The inaccuracy of these MDT pressure points were taken into account in the final pre-drill model of Prospect B.

Similar to Well A5, drillers experienced issues with overpressure in the formation close to the salt seal at 21,000 ft. The mud weight was raised too high and exceeded the fracture pressure. Many of the problems often occur around the salt seals. Several casings had to be placed relatively close to one another due to mud weight being too low or too high. In these areas of the well, the mud weight window is very narrow and can create difficulties with proper wellbore control if the pore pressure and fracture pressure models being used are not precise.

Bower's seismic interval velocity method, illustrated in Figure 24 and Figure 25, provided a reasonable pore pressure and fracture pressure model. The extent of accuracy is highly dependent on the quality of seismic data. Below the salt at 21,000 ft, the pore pressure gradient and fracture pressure gradient are 15 ppg and 15.75 ppg, respectively. Using Bower's model, at 29,000 ft, the pore pressure gradient is 16.6 ppg and the fracture pressure gradient is 17.75 ppg. Well B1 mud weight window below the salt ranges between 0.75 ppg and 1.25 ppg.

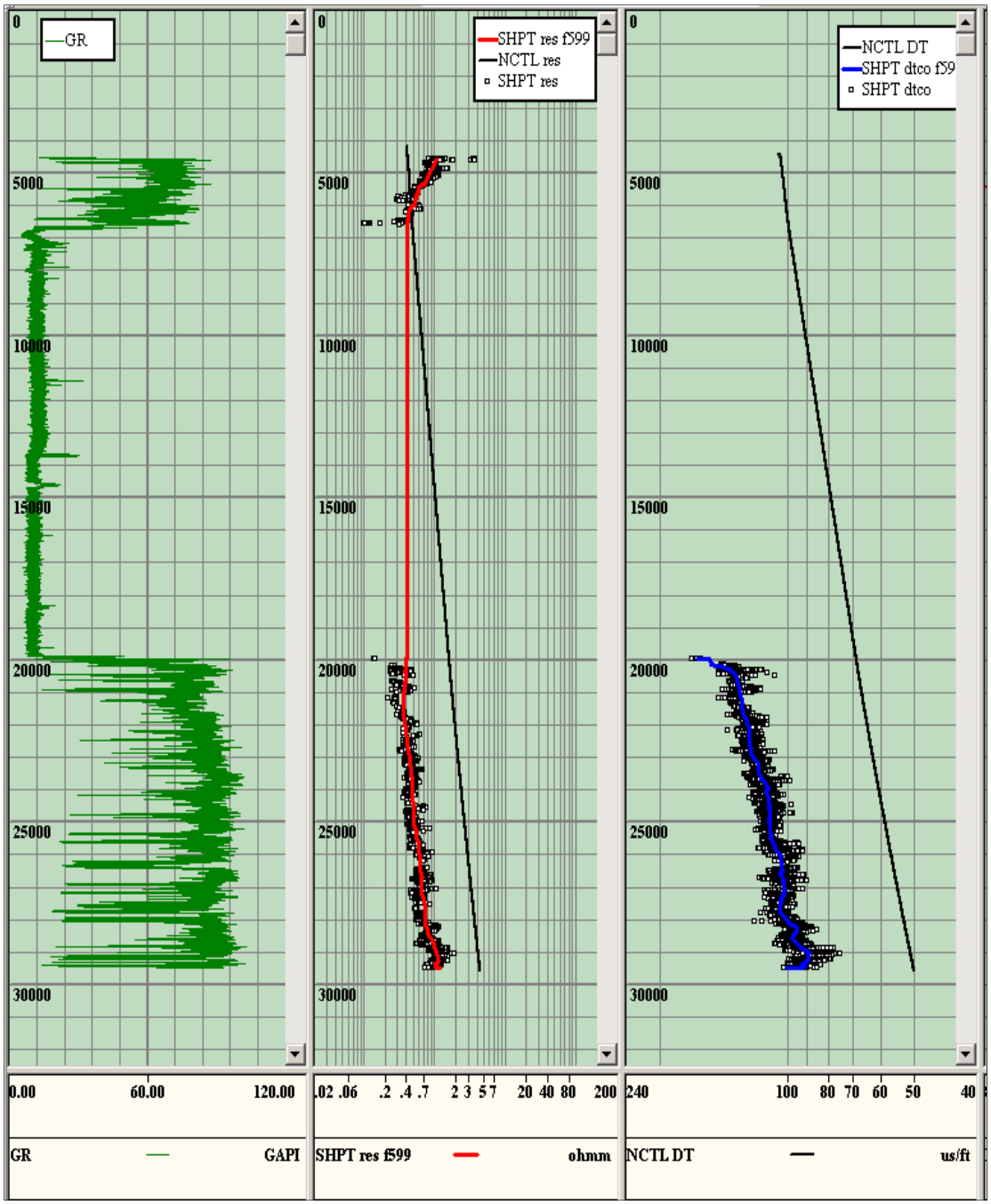

Figure 22. Shale point intervals and normal compaction trend of Eaton's resistivity and Eaton's sonic method for Well B1

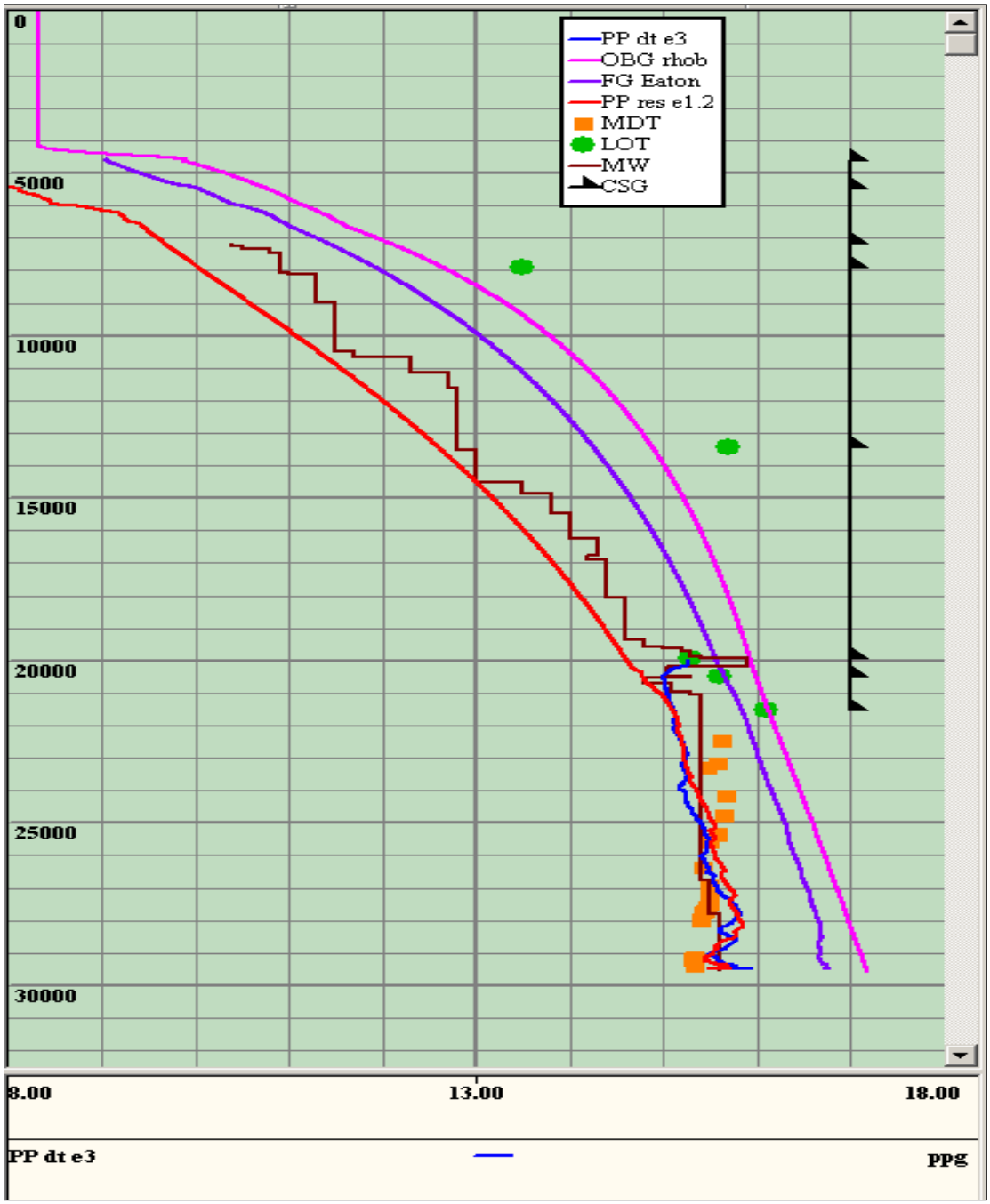

Figure 23. Calibrated pore pressure and fracture pressure models of Eaton's resistivity and Eaton's sonic method for Well B1

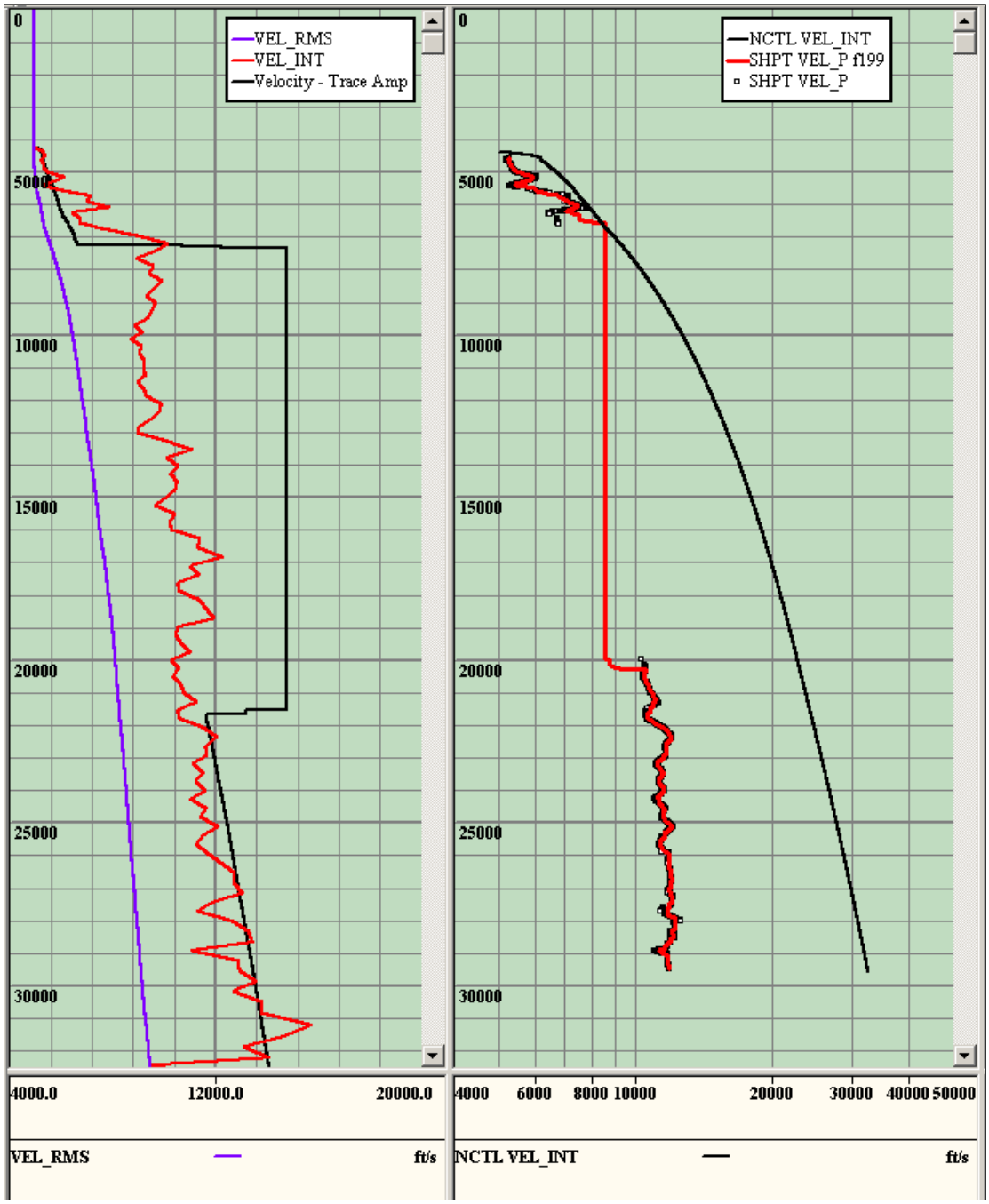

Figure 24. Seismic interval velocity and normal compaction trend of Bower's method for Well B1

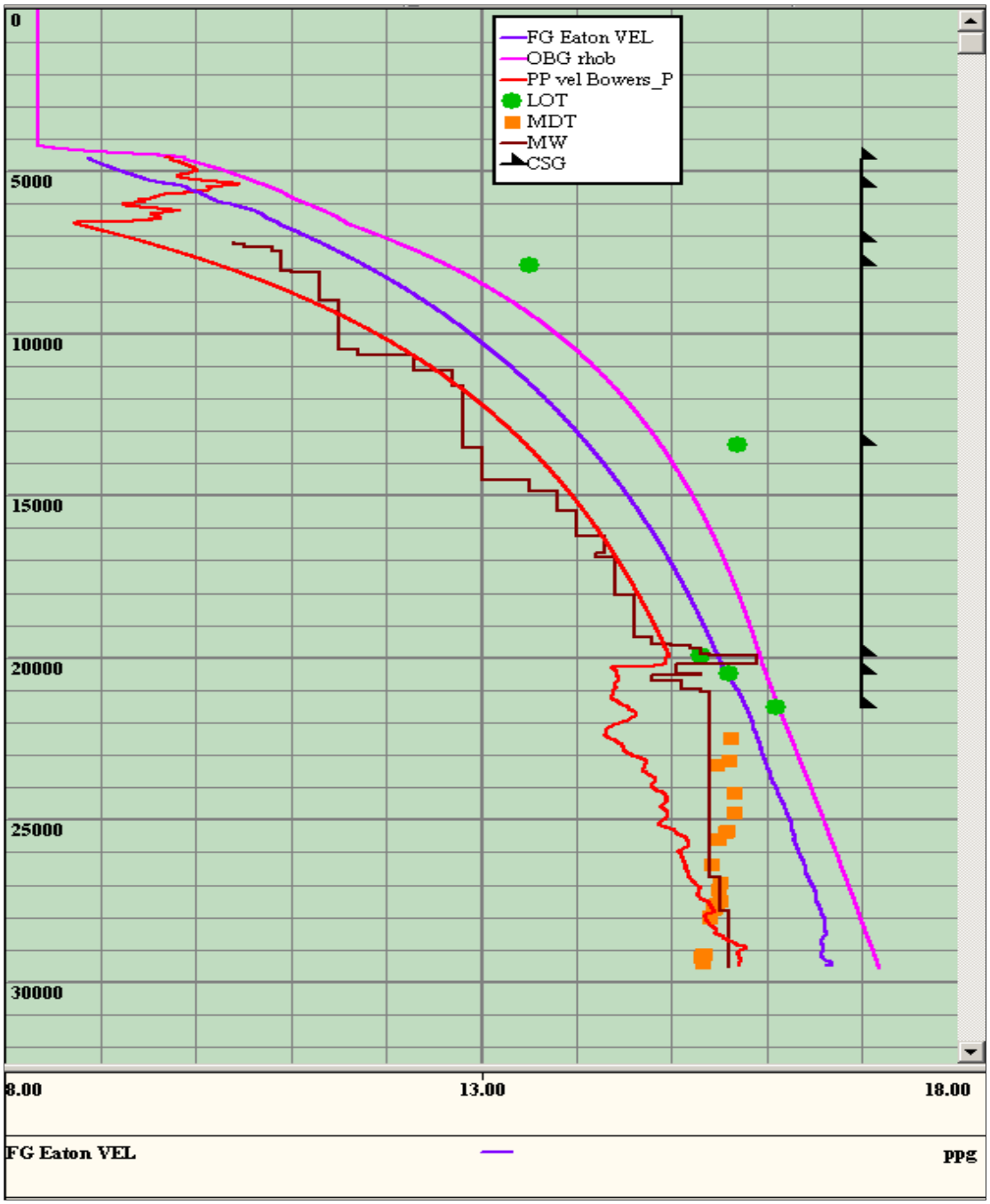

Figure 25. Calibrated pore pressure and fracture pressure model of Bower's seismic interval velocity method for Well B1

3.2.2 Offset Well B2

Well B2 was the only other usable offset well available to model pore pressure and fracture pressure for Prospect B. Figure 26 through Figure 29 displays the modeled results for each method. The quality of seismic interval velocity data proved to be too poor to use in the final pre-drill model. Displayed in Figure 28, the data can only be described as a "spiky mess". A smoothing effort was applied to the data to attempt a modeling procedure. However, the initial seismic interval velocity data was so heavily altered that it was no longer credible.

Eaton's resistivity and sonic methods, illustrated in Figure 26 and Figure 27, show a reasonable pore pressure and fracture pressure model using LWD data. Resistivity and sonic measurements were available for almost the entire well. At a depth of 20,000 to 21,000 ft, missing sonic measurements were synthetically generated using the gamma ray and resistivity logs, causing it to follow a similar pattern. As stated earlier, the most probably cause of resistivity increasing significantly below the salt seal is inaccurate tool response or salt diffusion.

The salt seal is located at a depth of 10,994 to 19,829 ft. Using the three methods and available drilling data, the pore pressure gradient and fracture pressure gradient immediately below the salt is 13.5 ppg and 15 ppg, respectively. At 29,000 ft, the pore pressure gradient is 14 ppg and the fracture pressure gradient is 16.5 ppg. These ranges are slightly lower than previous offset wells. Well B2 was not used to model the final pre-drill pore pressure and fracture pressure gradients of Prospect B.

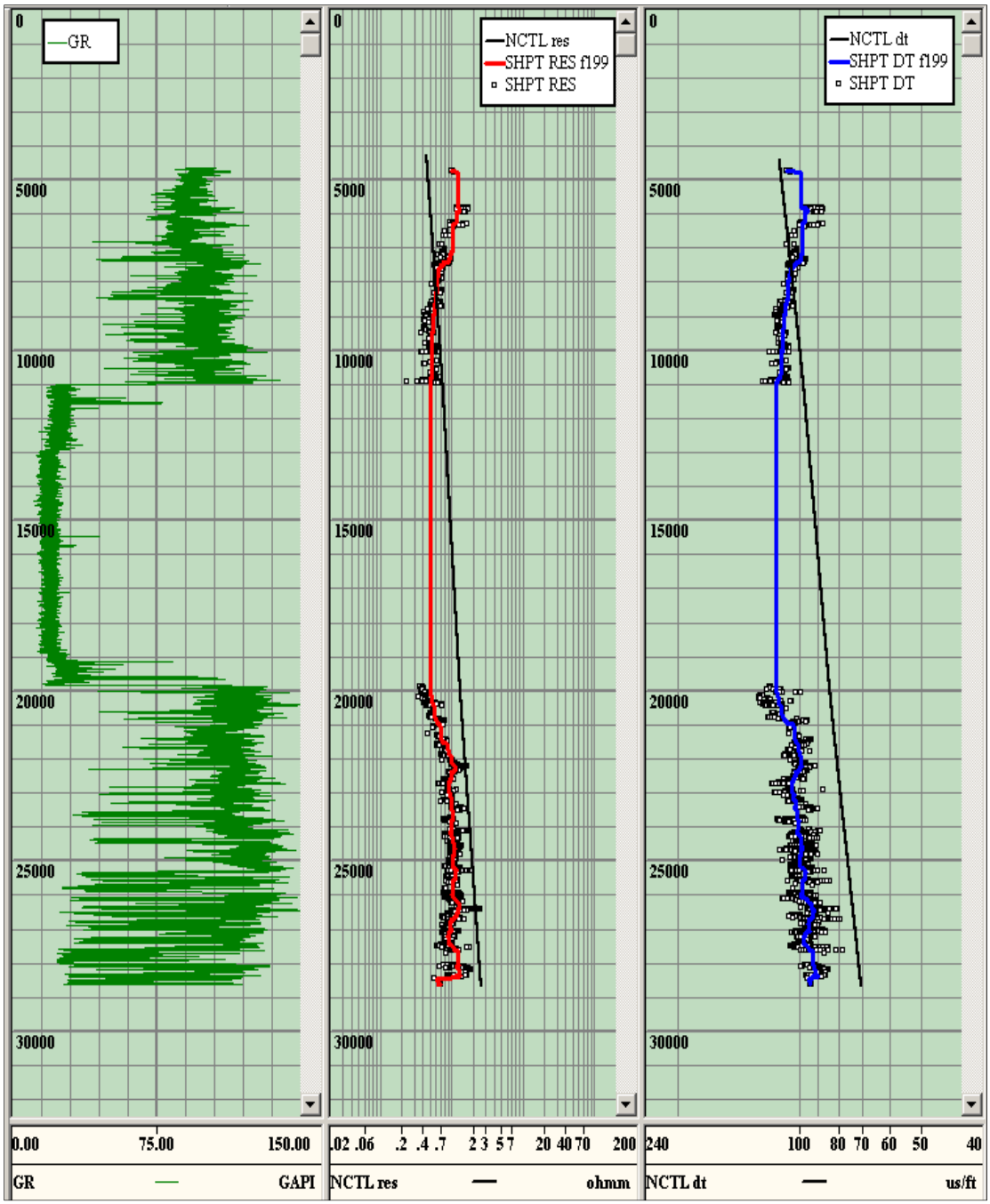

Figure 26. Shale point intervals and normal compaction trend of Eaton's resistivity and Eaton's sonic method for Well B2

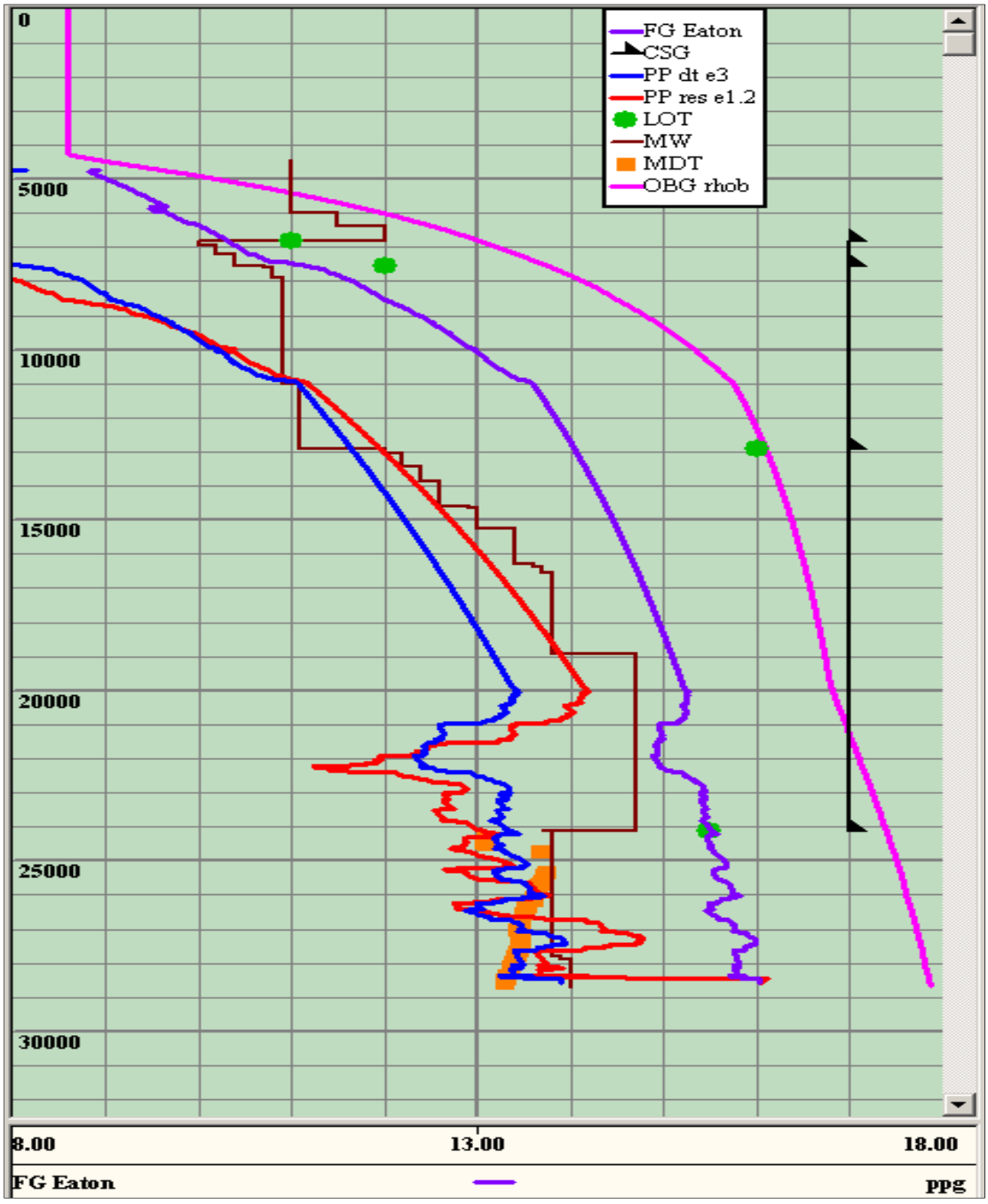

Figure 27. Calibrated pore pressure and fracture pressure models of Eaton's resistivity and Eaton's sonic method for Well B2

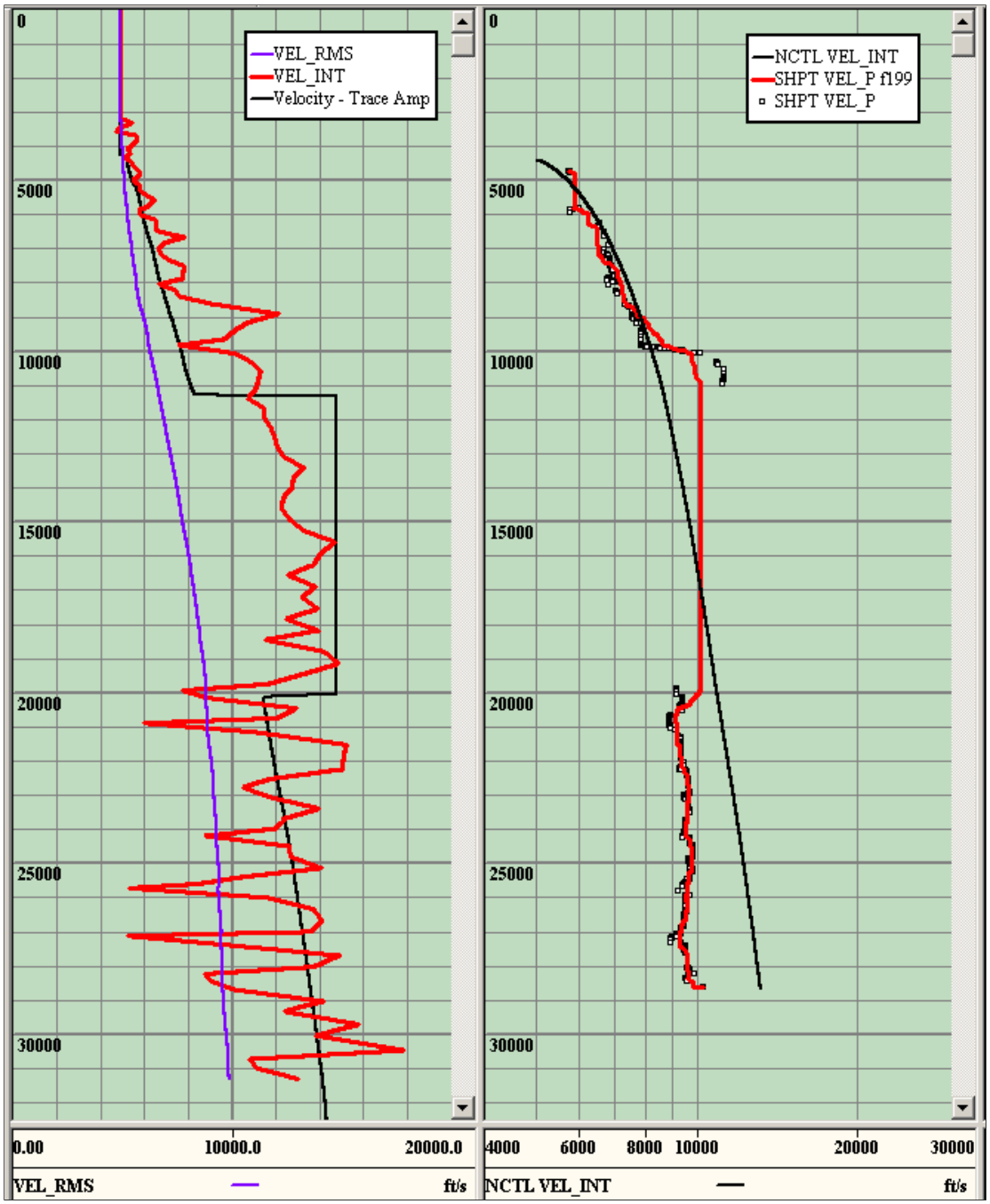

Figure 28. Seismic interval velocity and normal compaction trend of Bower's method for Well B2

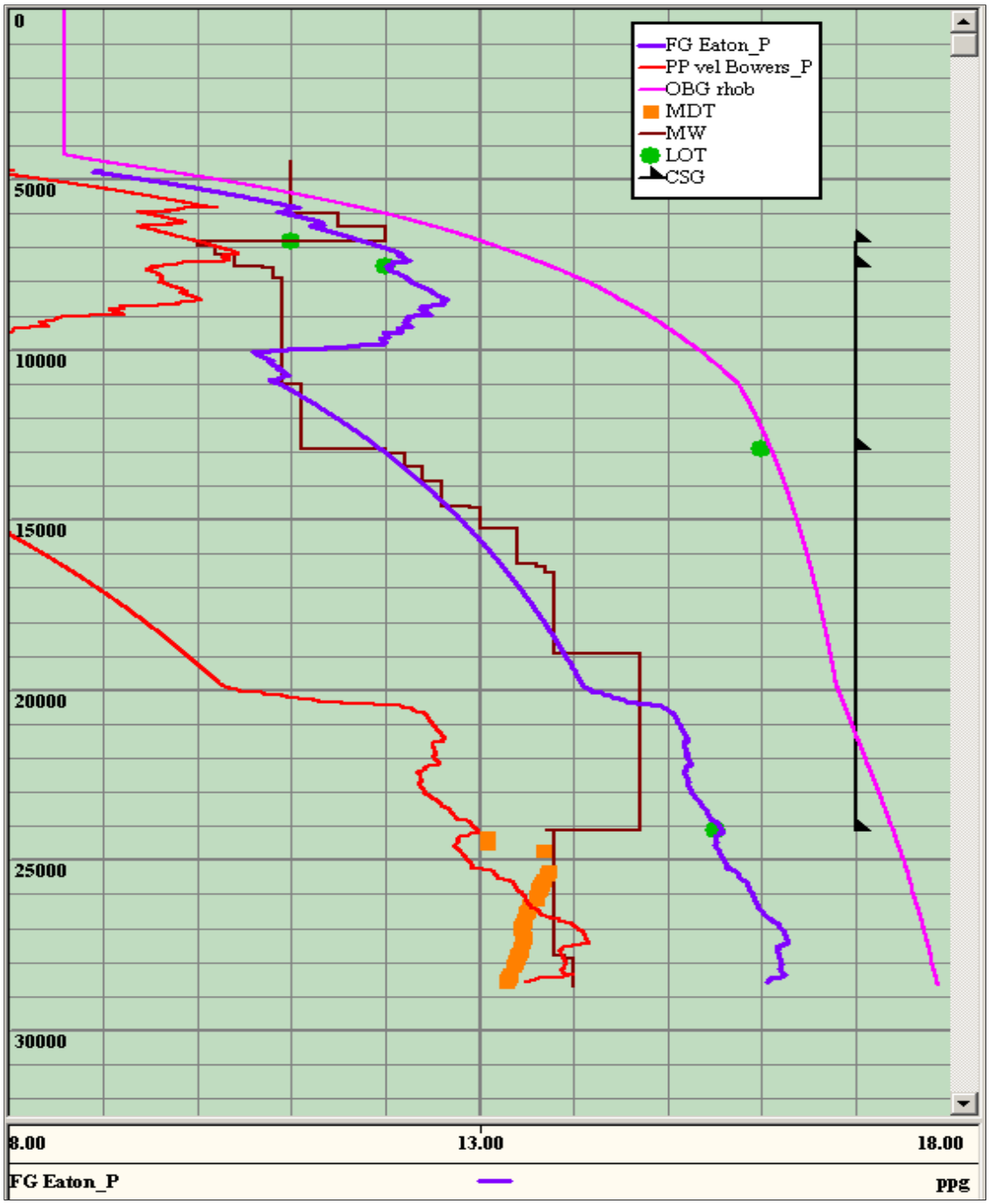

Figure 29. Calibrated pore pressure and fracture pressure model of Bower's seismic interval velocity method for Well B2

3.3 Prospect Wells

Seismic interval velocity logs are the only available logs for the two prospect wells. A separate bulk density curve was generated for each prospect well based on the bulk density logs for respective offset wells. This will be discussed in more detail in the next sections. Table 8 below provides a description of the two prospect wells.

Table 8: Description of prospect wells

	Water Depth	Salt Seal	TVD
	ft	ft	ft
Prospect A	2612	22567 - 23381	N/A
Prospect B	3395	8850 - 21480	N/A

Once a bulk density curve is generated for each prospect, overburden gradient can be calculated from the bulk density curve. Bower's method can then be applied to the seismic interval velocity data. Each well can be calibrated using respective offset well data: Bower's method compaction trend coefficients; MDT pressure points; LOT pressure points. Many other important aspects of offset wells need to be taken into account to finalize the design such as location and length of salt seals, water depths, geologic seismic data. The final pore pressure and fracture pressure models are highly based on user interpretation.

3.3.1 Prospect Well A Model

Five offset wells were used in the final study of pore pressure and fracture pressure of Prospect A. A synthetic bulk density curve for Prospect A was manually

created using offset well bulk density data, illustrated in Figure 30; Equation 3.1 was used.

$$\text{Bulk Density} = 0.194 * \ln(\text{TVD} - \text{WD}) + 0.58 \quad (7)$$

Where,

WD = Water depth

TVD = Total vertical depth

Figure 30 shows the smoothing effect that was applied to Prospect A seismic interval velocity data. The extent of the smoothing was based on the offset wells. Figure 32 displays the final pore pressure and fracture pressure model of Prospect A. Bower's method normal compaction trend coefficients A and B were set to 14.15 and 0.75, respectively. Offset well coefficients ranged from 14 to 14.2 for A and 0.713 to 0.754 for B. MDT pressure points and LOT pressure points were depth-corrected using the water depth of Prospect A and offset wells. Final mud weight window ranged from 1 ppg to 2 ppg, averaging 1.5 ppg.

Table 9 and Table 10 show the proposed mud weight and casing designs for Prospect A based on final pore pressure and fracture pressure models. A total of eight casing sizes were proposed for Prospect A to accommodate the pore pressure and fracture pressure window.

Table 9: Proposed mud weight design for Prospect A

TVD,	MW	MW
ft	ppg	psi
5800	11.8	3555.5
7900	11.8	4842.8
7900.01	12.71	5216.3
11800	12.71	7791.4
11800.01	14.3	8766.1
16317	14.3	12121.7
16317.01	15.45	13096.5
23000	15.45	18460.4
23000.01	15.81	18890.6
25200	15.81	20697.5
25200.01	16.85	22059.0

Table 10: Proposed casing design for Prospect A

TVD	CSG
ft	in
3200	36
4100	28
5000	22
7900	17.875
11800	16
16317	13.625
23000	9.875
25200	7.625

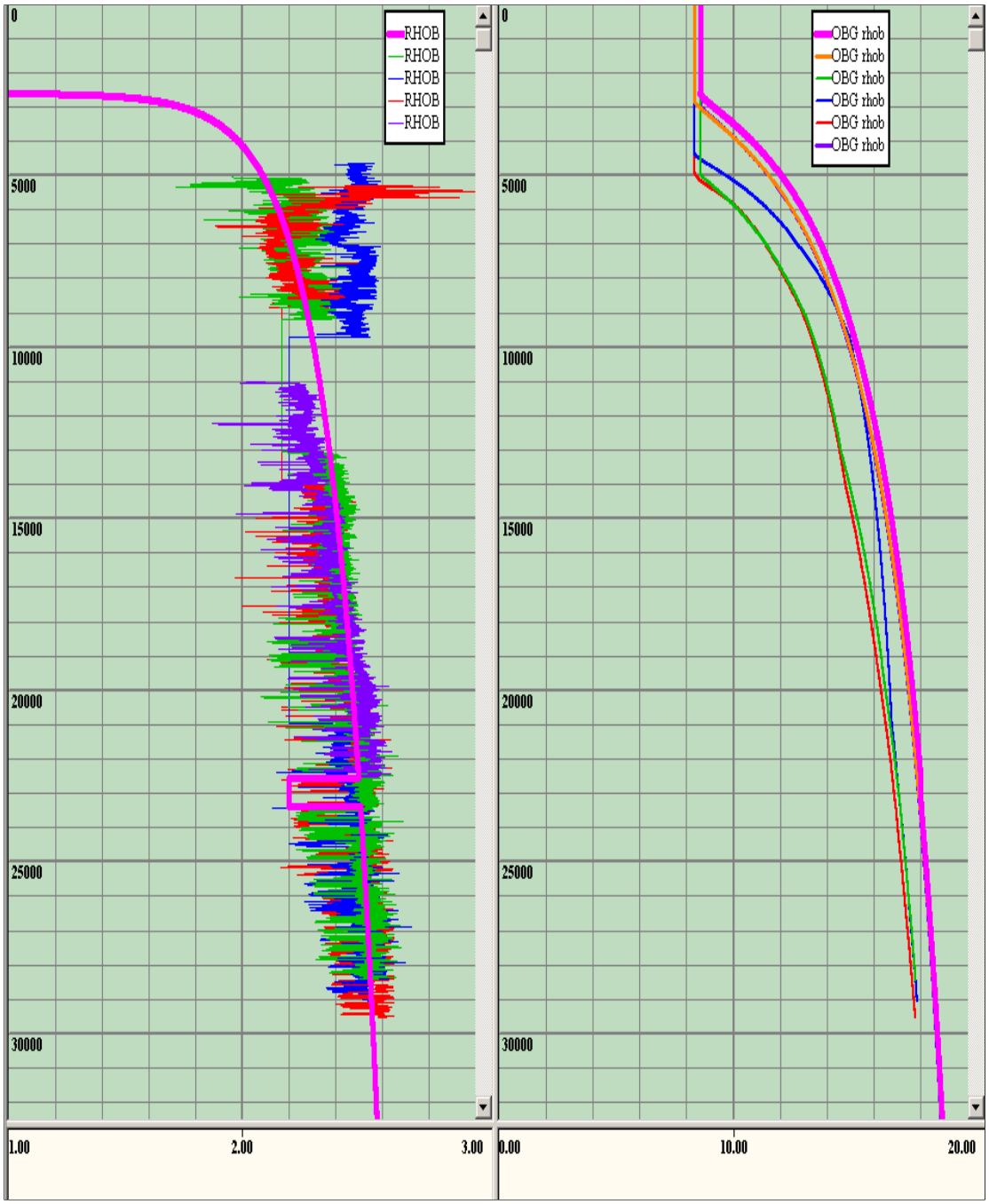

Figure 30. Synthetic bulk density curve for Prospect A and offset well bulk density.

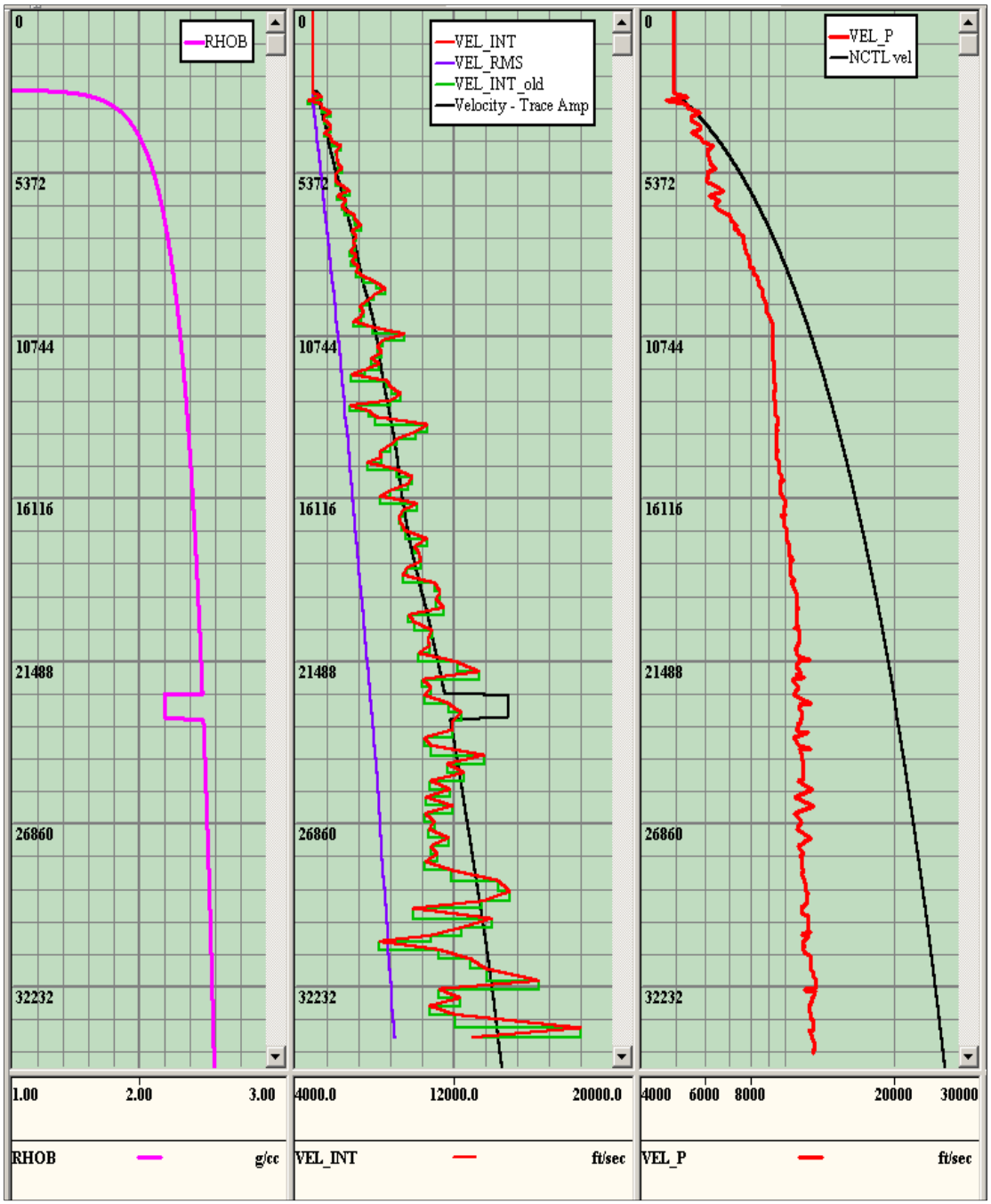

Figure 31 Generated bulk density, seismic interval velocity, and normal compaction trend of Bower's method for Prospect A

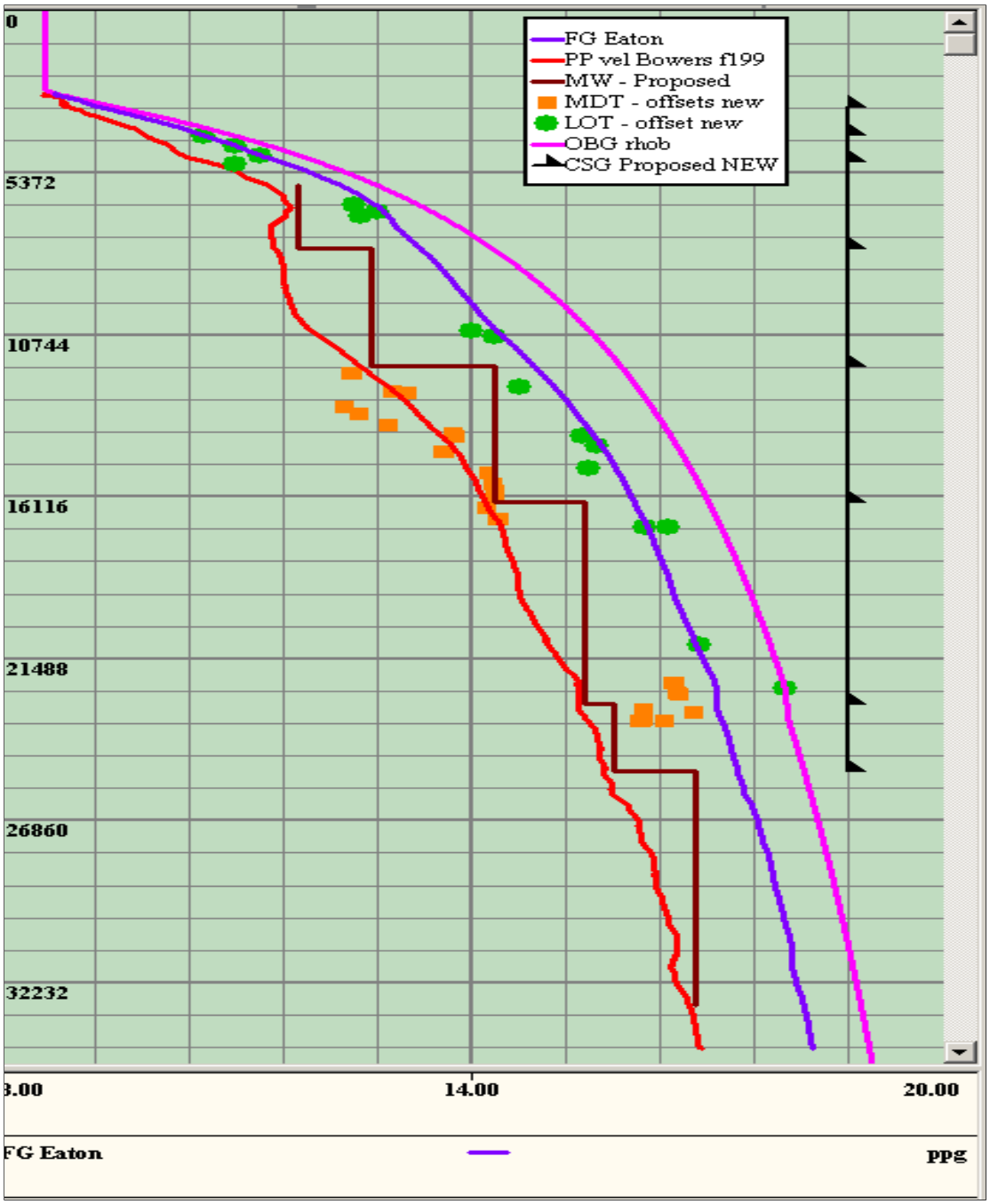

Figure 32. Final pore pressure and fracture pressure model of Bower's seismic interval velocity method for Prospect A

3.3.2 Prospect Well B

Well B1 was the only well used in the study of pore pressure and fracture pressure for Prospect B. The synthetic bulk density equation for Prospect B is displayed below.

$$\text{Bulk Density} = 0.18 * \ln(\text{TVD} - \text{WD}) + 0.675 \quad (8)$$

Where,

WD = Water depth

TVD = Total vertical depth

Similar to Prospect A, seismic interval velocity is smoothed to favor shale intervals, illustrated in Figure 35. Bower's normal compaction trend coefficients A and B were set to 14.5 and 0.8, respectively. Offset well, or Well B1, coefficients were 14.75 for A and 0.8 for B. Prospect B has a larger salt seal and therefore requires less casings. In each offset well for both prospects, typically only one casing point was set in the salt seal. Below the salt seal, Prospect B mud weigh window averages 1.25 ppg, which is smaller than Prospect A. Prospect B mud weight window ranges from 1 ppg to 1.75 ppg.

Table 11 and Table 12 exhibit the proposed mud weight and casing designs for Prospect B. Five casing points are used in the casing design. Although the mud weight windows of Prospect A and Prospect B are similar in size, Prospect B has a larger salt seal and therefore requires less casing points.

Table 11: Proposed mud weight design for Prospect B

TVD	MW	MW
ft	ppg	psi
8149	12.5	5291.8
20300	12.5	13182.3
20300.01	15.05	15871.5
23550	15.05	18412.5
23550.01	15.85	19391.3
28100	15.85	23137.8
28100.01	16.6	24232.6

Table 12: Proposed casing design for Prospect B

TVD	CSG
ft	in
5588	28
6729	22
20300	17.875
23550	13.625
28100	9.625

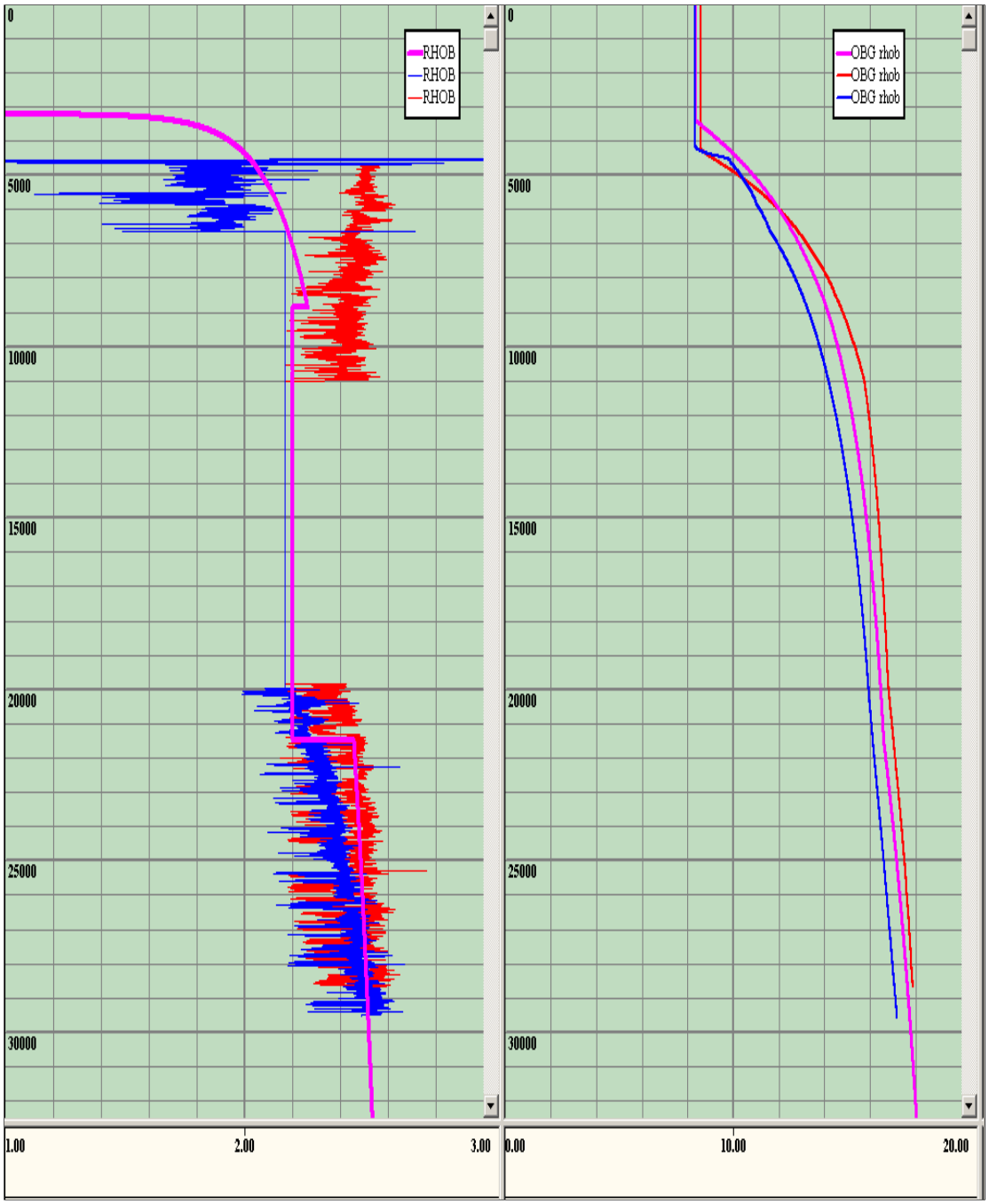

Figure 33. Synthetic bulk density curve for Prospect B and offset well bulk density.

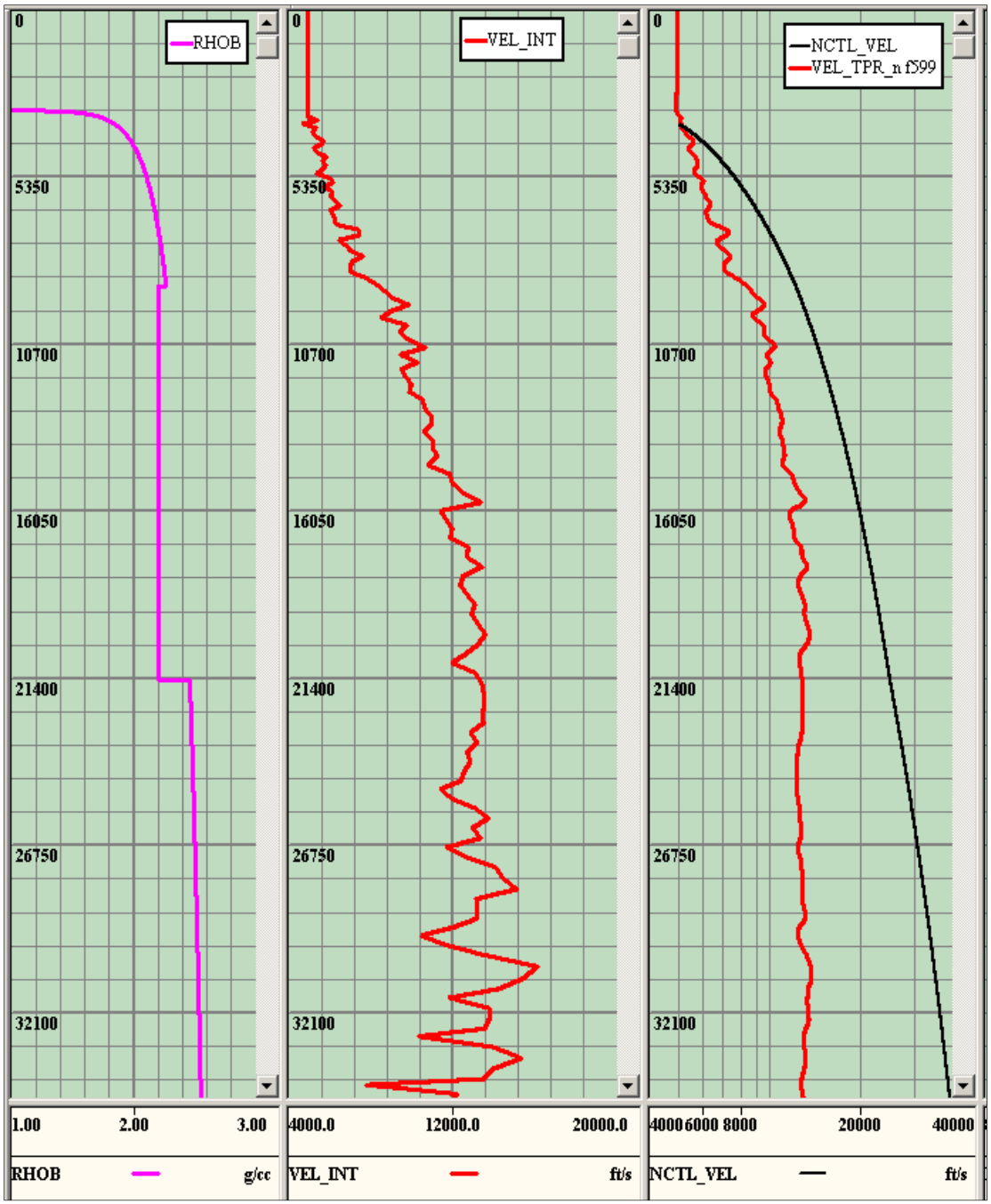

Figure 34. Generated bulk density, seismic interval velocity, and normal compaction trend of Bower's method for Prospect B

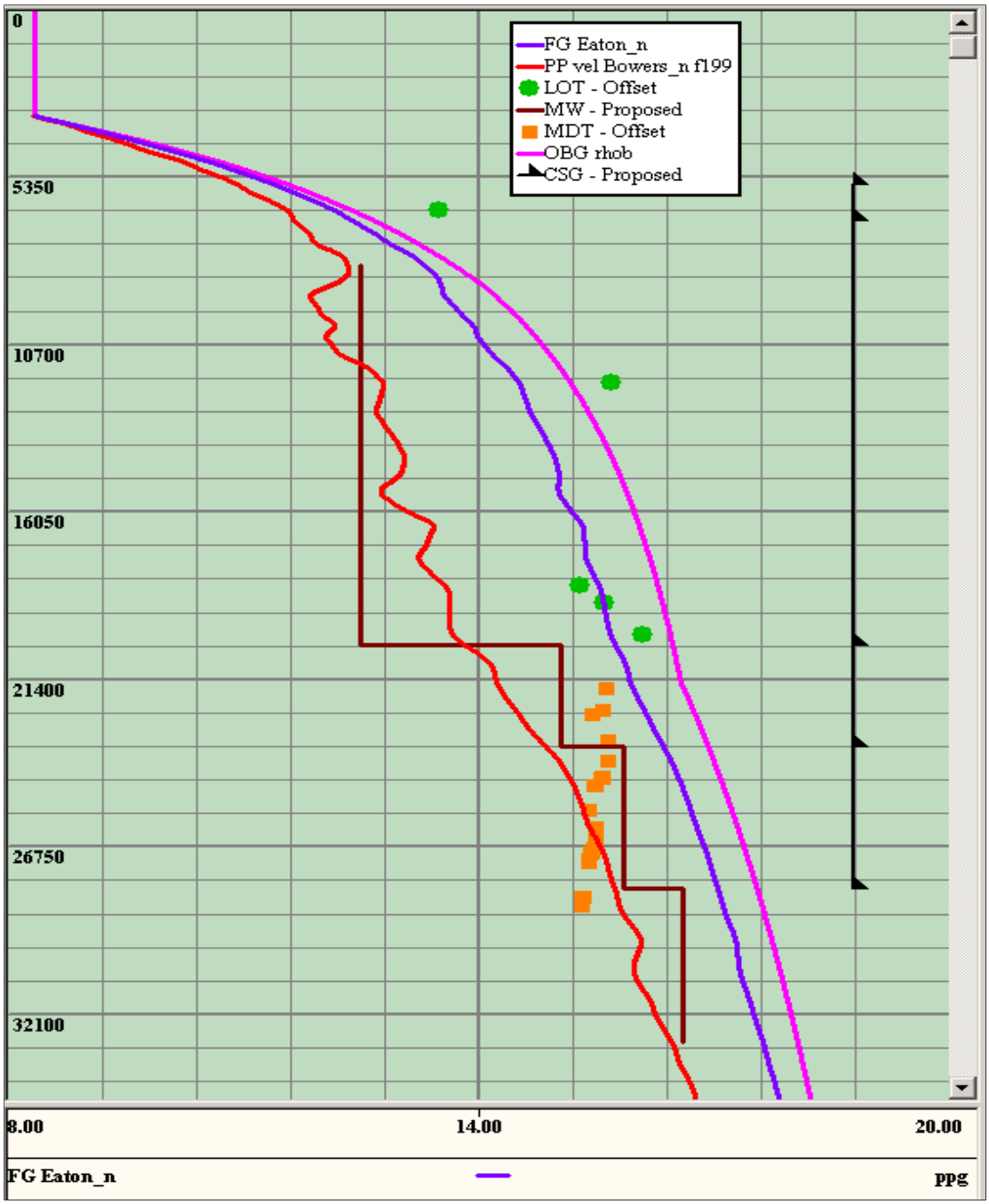

Figure 35. Final pore pressure and fracture pressure model of Bower's seismic interval velocity method for Prospect B

CHAPTER 4: CONCLUSIONS AND FUTURE WORK

In this chapter, the results and conclusions observed from pore pressure and fracture pressure predictions for offset and prospect wells will be summarized. Five pore pressure and fracture pressure models were created for Prospect A and two were created for Prospect B. Eaton's resistivity and sonic methods will be used for real-time drilling pore pressure and fracture pressure analysis. Eaton's seismic method was modeled to create pre-drill pore pressure and fracture pressure models for the two prospect wells.

4.1 Summary of Offset Wells

- Salt diffusion affected the resistivity log and in result provided incorrect estimations of pore pressure for depths immediately below salt seal. Well A2 and A5 were affected. Eaton's resistivity method for these sections were ignored.
- MDT, LOT, and mud weight drilling data agreed with pore pressure and fracture pressure models. This suggested that offset wells were grouped correctly and Eaton's resistivity and sonic methods were working properly.
- Eaton's seismic method matched Eaton's resistivity and sonic methods.
- Mud weight windows for all offset wells were tight: ranging from 1 to 2 ppg. Pore pressure and fracture pressure gradients followed similar patterns. However, exact pore pressure and fracture pressure depended on many factors: depth, salt size and location, water depth, geologic location, and accuracy of available data.

- Casing designs ranged from six to eight casing points depending on size of salt and depth of well.

4.2 Summary of Prospect Wells

- Synthetic bulk density curve was created using offset well bulk density logs. Equation 3.1 and Equation 3.2 were used for Prospect A and Prospect B, respectively.
- Seismic interval velocity for prospect wells was smoothed to favor shales in a similar manner to the offset wells. LWD logs were used to evaluate speeds of shale formations to see whether or not they were slower or faster than sand formations.
- Prospect wells mud weight windows ranged from 1 to 2 ppg, averaging 1.5 ppg. Similar to the offset wells, the exact pore pressure and fracture pressure depends highly on many factors such as: depth, salt size and location, water depth, geologic location, and accuracy of available data.
- Mud weight design and casing design depend on size of mud weight window and salt seal. Mud weight and casing design can be found in Table 9 through Table 12.

4.3 Recommendations and Future Work

- In many cases, Eaton's sonic method exhibited a better pore pressure prediction response. It is recommended to have accurate sonic log measurements for future pore pressure and fracture pressure models.
- Being aware of the effects of salt diffusion can benefit real-time monitoring of drilling and pore pressure estimation. Resistivity logs can also help find salt seals if drillers are unaware of their location.
- Seismic interval velocity is one of the only tools used in pre-drill pore pressure and fracture pressure modeling. "Spiky" or messy seismic data may need to be reprocessed in order to attain a precise pore pressure and fracture pressure model.
- Eaton's resistivity and sonic method compaction trend coefficients will be used to monitor and calibrate real-time pore pressure and fracture pressure estimations.

APPENDICES

The mud weight drilling data, LOT pressure points, MDT pressure points, and casing points are represented below for each offset well. This data was taken from drilling data files and manually inputted into Excel and PPredict to calibrate pore pressure and fracture pressure models.

A. Data for Offset Wells

A.1 Offset Well A1

Table 13. Mud weight drilling data of Well A1

MD From	MD To	TVD From	TVD To	MW
ft	ft	ft	ft	ppg
7670	8220	7669	8219	10.3
8220	9020	8219	9018	10.4
9020	9400	9018	9398	10.5
9400	11920	9398	11915	11.3
11920	12320	11915	12315	11.4
12320	12700	12315	12694	11.3
12700	13525	12694	13517	11.3
13525	13920	13517	13911	11.3
13920	15140	13911	15128	12.6
15140	15200	15128	15187	13.0
15200	15920	15187	15906	13.1
15920	16740	15906	16725	13.2
16740	17931	16725	17915	13.2
17931	18520	17915	18503	13.7
18520	18940	18503	18922	13.8
18940	19750	18922	19728	13.8
19750	20520	19728	20490	13.9
20520	21020	20490	20984	14.0
21020	21800	20984	21757	14.1
21800	22160	21757	22116	14.0
22160	22600	22116	22554	14.1
22600	23820	22554	23769	14.1
23820	25650	23769	25591	14.2
25650	26320	25591	26258	14.0
26320	27100	26258	27036	13.8
27100	28700	27036	28630	14.3

Table 14. Leak-off test drilling data of Well A1

MD	TVD	LOT
ft	ft	ppg
7498	7497	10.9
9347	9345	13.0
13525	13517	14.2
17931	17915	14.8
22160	22116	15.6
25246	25187	15.8

Table 15. MDT drilling data of Well A1

TVD	MDT
feet	ppg
22318.44	12.838
22580.47	12.892
22697.22	12.875
22786.87	12.858
22788.82	12.865
23493.94	13.975
23495.83	13.970
23771.47	13.910
23773.54	13.915
23836.29	13.897
23948.67	13.874
24216.02	13.818
24337.23	13.793
24700.3	13.686
24776.95	13.669
25107.77	13.617
25160.51	13.606
25309.68	13.587
26161.12	14.820
26465.82	13.854
26910.49	14.207
26939.38	14.452
27353.1	14.530
27386.12	14.516
27611.31	14.381
27669.07	14.367
27704.17	14.358
27742.79	14.351
27863.82	14.334
27884.71	14.321
27905.58	14.323
28230.57	14.339
28248.49	14.307
29137.27	14.650
29159.24	14.641
29398.71	14.796
29410.55	14.793
29427.97	14.793
29435.47	14.791
29444.42	14.798
29446.39	14.802

Table 16. Casing points of Well A1

MD	TVD	Casing
ft	ft	in
5264	5263.9	36
5963	5962.9	28
7498	7497.55	22
9347	9345.25	17.875
13525	13517.97	16
17931	17915.28	13.375
22160	22116.52	11.875
25246	25187.99	9.625

A.2 Offset Well A2

Table 17. Mud weight drilling data of Well A2

MD To	TVD From	TVD To	MW
feet	feet	feet	ppg
5975	5543.92	5974.84	11.5
6800	5974.84	6799.76	12
7225	6799.76	7224.71	12.5
7250	7224.71	7250.21	12.7
7257	7250.21	7256.71	13
8962	7256.71	8961.57	10.5
10000	8961.57	9999.55	10.7
12325	9999.55	12324.31	10.7
12515	12324.31	12513.75	10.9
13080	12513.75	13073.32	11.2
14420	13073.32	14355.63	11.7
14875	14355.63	14766.66	12
15100	14766.66	14966.20	12.3
16115	14966.20	15831.56	12.8
16750	15831.56	16391.14	13.1
18150	16391.14	17603.12	13.4
20110	17603.12	19345.22	13.6
20770	19345.22	19946.32	13.8
22150	19946.32	21171.19	14.1

Table 18. Leak-off test drilling data of Well A2

MD	TVD	LOT
feet	feet	ppg
7259	7258.71	10.9
8962	8961.57	12.1
11422	11421.54	15.1
17955	17436.62	16
24258	23003.32	15.7
26285	24816.03	15.7

Table 19. MDT drilling data of Well A2

TVD	MDT
ft	ppg
24488.71	13.854
24497.7	13.851
24506.69	13.848
24515.82	13.845
24524.82	13.841
23416.65	14.648
23420.22	14.645
23416.6	14.646
24439.9	13.870
24434.59	13.872
24400.11	13.884
24405.51	13.882
24420.04	13.877
24423.62	13.875
24432.56	13.873
24441.67	13.870
24439.95	13.870
24452.57	13.866
24461.63	13.863
24470.61	13.860
24479.75	13.857

Table 20. Casing points of Well A2

MD	TVD	Casing
ft	ft	in
7259	7258.71	22
8962	8961.57	18
11422	11421.54	16
17955	17436.62	13.625
24258	23003.32	11.875
26285	24816.03	9.625

A.3 Offset Well A3

Table 21. Mud weight drilling data of Well A3

MD From	MD To	TVD From	TVD To	MW
feet	feet	feet	feet	ppg
8102	9000	8101.56	8999.51	10.1
9000	9207	8999.51	9206.50	10.2
9207	13750	9206.50	9950.00	10.3
13750	13925	9950.00	13783.51	13
13925	15300	13783.51	15049.82	13
15300	15750	15049.82	15468.95	13.1
15750	16250	15468.95	15930.68	13.2
16250	17100	15930.68	16715.64	13.3
17100	18276	16715.64	17802.00	13.4
18276	18400	17802.00	17916.22	13.5
18400	18500	17916.22	18008.59	13.5
18500	19707	18008.59	19123.53	13.8
19707	25500	19123.53	24514.63	14
25500	25600	24514.63	24560.88	14.1
25600	26100	24560.88	25023.15	14.3
26100	27725	25023.15	26528.38	14.5
27725	29275	26528.38	27954.64	14.6
29275	30550	27954.64	29128.16	14.7

Table 22. Leak-off test drilling data of Well A3

MD	TVD	LOT
feet	feet	ppg
8102	8101.56	11
9821	9820.47	14.3
15085	14851.18	13.8
18276	17801.54	14.7
25378	24355.56	15.7

Table 23. MDT drilling data of Well A3

TVD	MDT
feet	ppg
19253.73	13.819
19309.37	13.805
20213.37	13.239
20215.39	13.238
20492.22	13.041
20501.91	13.037
20921.87	14.317
20922.84	14.318
20927.56	14.318
20931.14	14.317
21116.7	12.959
21122.06	12.959
22270.9	12.847
22296.5	12.840
22318.37	12.839
22475.56	12.927
22483.78	12.925
22576.97	12.904
22620.41	12.903
23582.32	13.965
23628.13	13.955
23674.19	13.944
23729.28	13.935
23755.09	13.929
23780.63	14.354
24072.6	13.861
24092.2	13.854
24109.64	13.844
24174.45	13.807
24182.29	13.806
24184.69	13.804
24186.18	13.614
24186.44	13.803
24205	14.322
24236.95	13.791
24237.32	13.792
24285.45	13.495
24288.59	13.781

TVD	MDT
feet	ppg
24294.52	13.778
24337.88	13.769
26975.09	14.537
26986.1	14.533
27003.79	14.526
27009.04	14.526
27015.16	14.524
27027.24	14.520
27037.96	14.516
27046.7	14.514
27071.05	14.507
27078.48	14.506
27086.7	14.503
27094.64	14.501
27178.91	14.484
27191.55	14.481
27241.96	14.473
27266.64	14.466
27278.71	14.464
27424.52	14.507
27429.41	14.505
27449.5	14.498
27458.75	14.487
27458.83	14.496
27538.61	14.470
27542.18	14.472
27547.81	14.469
27551.46	14.468
27560.87	14.464
27574.7	14.461
27588.67	14.457
27596.98	14.455
27606.28	14.454
27796.26	14.484
27811.91	14.480
27862.5	14.463
27867.1	14.464

Table 24. Casing points of Well A3

MD	TVD	Casing
feet	feet	in
5371	5371	38
8102	8101.56	22
9821	9820.47	18
15085	14851.18	16
18276	17801.54	13.625
25378	24355.56	11.875

A.4 Offset Well A4

Table 25. Mud weight drilling data of Well A4

MD From	MD To	TVD From	TVD To	MW
ft	ft	ft	ft	ppg
3360	4399	3359	4398	8.6
4399	5056	4398	5055	8.6
5056	5084	5055	5083	10.3
5084	6104	5083	6103	10.4
6104	6953	6103	6952	10.4
6953	7333	6952	7331	10.8
7333	10077	7331	10075	11.2
10077	11027	10075	11025	12.2
11027	11228	11025	11226	12.4
11228	14380	11226	14377	13
14380	16335	14377	16332	13.7
16335	17369	16332	17366	14
17369	18492	17366	18488	14.4
18492	19814	18488	19810	14.4
19814	22500	19810	22496	14.5

Table 26. Leak-off test drilling data of Well A4

TVD	LOT
ft	ppg
4387	10.6
5041	11.3
6873	12.8
11024	14.3
14332	15.4
17368	16.5

Table 27. MDT drilling data of Well A4

TVD	MDT
ft	ppg
12225.58	12.478
12238.06	12.457
12242.03	12.490
12827.53	12.993
12866.96	13.173
13361.98	12.388
13574.09	12.554
13953.19	12.940
13962.01	12.936
13969.95	12.933
14210.03	13.752
14307.08	13.784
14828.1	13.645
14841.04	13.634
15552.2	14.212
15889.18	14.259
16135.22	14.290
16261	14.299
17060.07	14.319
17068.15	14.352
16677.27	14.174
14828.1	13.645
14841.04	13.634
15552.2	14.212
15889.18	14.259
16135.22	14.290
16261	14.299
17060.07	14.319
17068.15	14.352
16677.27	14.174

Table 28. Casing points of Well A4

TVD	CSG
ft	ppg
3141	36
4387	20
5041	16
6873	13.375
11024	11.75
14332	9.625
17368	7.625

A.5 Offset Well A5

Table 29. Mud weight drilling data of Well A5

MW From	MW To	TVD From	TVD To	MW
ft	ft	ft	ft	ppg
6783	10963	6782	10960	10.7
10963	13346	10960	13342	12.1
13346	15525	13342	15519	13.3
15525	20907	15519	20899	14.4
20907	21520	20899	21508	14.5
21520	21672	21508	21660	15.7
21672	22592	21660	22579	16.2
22592	23950	22579	23936	16.6
23950	24964	23936	24950	16.5
24964	26569	24950	26555	16.4

Table 30. Leak-off test drilling data of Well A5

TVD	LOT
ft	ppg
4802	11
6761	12.5
10932	14
14731	15.6
21342	16.9
22786	18

Table 31. MDT drilling data of Well A5

TVD	MDT
ft	ppg
22955.13	16.64414
22956.08	16.64371
22933.01	16.60421
22610.1	16.56342
22595.24	16.57131
22607.13	16.56779
23819.62	16.17347
23837.46	16.14315
23845.65	16.14017
23871.45	16.44937
23820.4	16.1726
23836.67	16.14628
23597.86	16.80859
23596.81	16.80884
23493.89	16.18726

Table 32. Casing points of Well A5

TVD	CSG
ft	in
3201	36
4023	28
4802	22
6761	17.875
10932	16
14731	13.625
21342	11.875
22590	9.875

A.6 Offset Well B1

Table 33. Mud weight drilling data of Well B1

MD From	MD To	TVD From	TVD To	MW, ppg
ft	ft	ft	ft	ppg
7180	7240	7179.8828	7239.8818	10.4
7240	7320	7239.8818	7319.8794	10.5
7320	7450	7319.8794	7449.8618	10.8
7450	7920	7449.8618	7919.3677	10.9
7920	8050	7919.3677	8049.3037	10.9
8050	8110	8049.3037	8109.2988	11
8110	8990	8109.2988	8989.2988	11.3
8990	9990	8989.2988	9989.2988	11.5
9990	10490	9989.2988	10489.2988	11.5
10490	10660	10489.2988	10659.2988	11.7
10660	11120	10659.2988	11119.2988	12.3
11120	11610	11119.2988	11609.2979	12.7
11610	13510	11609.2979	13509.2979	12.8
13510	14510	13509.2979	14509.2969	13
14510	14840	14509.2969	14839.2969	13.5
14840	15470	14839.2969	15469.2949	13.8
15470	16225	15469.2949	16224.291	14
16225	16775	16224.291	16774.2871	14.3
16775	16910	16774.2871	16909.2852	14.2
16910	18070	16909.2852	18069.2754	14.4
18070	19340	18069.2754	19339.2285	14.6
19340	19580	19339.2285	19579.207	14.8
19580	19630	19579.207	19629.2031	15
19630	19700	19629.2031	19699.1992	15.2
19700	19900	19699.1992	19899.166	15.3
19900	19920	19899.166	19919.1602	15.4
19920	19940	19919.1602	19939.1504	15.8
19940	20190	19939.1504	20188.9492	15.9
20190	20475	20188.9492	20473.7051	15.05
20475	20525	20473.7051	20523.6699	15.3
20525	20685	20523.6699	20683.5684	14.8
20685	20980	20683.5684	20978.4375	15.1
20980	21040	20978.4375	21038.4238	15.3
21040	26990	21038.4238	26764.3633	15.4
26990	28090	26764.3633	27812.668	15.5
28090	29900	27812.668	29525.1387	15.6

Table 34. Leak-off test drilling data of Well B1

TVD	LOT
ft	ppg
7910	13.5
13454	15.7
19931	15.3
20470	15.6
21508	16.1

Table 35. MDT drilling data of Well B1

TVD	MDT
ft	ppg
22472	15.62
23153	15.60
23289	15.47
23293	15.47
23297	15.46
24147	15.66
24773	15.66
25319	15.58
25338	15.58
25363	15.57
25587	15.49
25596	15.49
25600	15.49
26356	15.42
26916	15.50
27163	15.50
27514	15.50
27585	15.47
27705	15.45
27723	15.44
27759	15.44
27948	15.40
28024	15.40
29136	15.33
29137	15.34
29177	15.32
29210	15.31
29398	15.33
29402	15.33

Table 36. Casing points of Well B1

TVD	CSG
ft	in
4588	36
5479	28
7154	22
7910	17.875
13454	16
19931	13.625
20471	11.875
21508	9.625

A.7 Offset Well B2

Table 37. Mud weight drilling data of Well B2

MD From	MD To	TVD From	TVD To	MW
ft	ft	ft	ft	ppg
4450	6000	4450	6000	11
6000	6400	6000	6400	11.5
6400	6812	6400	6812	12
6812	6950	6812	6950	10
6950	7200	6950	7200	10.2
7200	7350	7200	7350	10.4
7350	7548	7350	7548	10.4
7548	7600	7548	7600	10.7
7600	7900	7600	7900	10.8
7900	9600	7900	9599	10.9
9600	11000	9599	10999	10.9
11000	11100	10999	11099	11.1
11100	12400	11099	12399	11.1
12400	12910	12399	12909	11.1
12910	13050	12909	13049	12
13050	13350	13049	13349	12.2
13350	13450	13349	13449	12.2
13450	13850	13449	13848	12.4
13850	14600	13848	14597	12.6
14600	14650	14597	14646	12.9
14650	15250	14646	15245	13
15250	15950	15245	15944	13.4
15950	16300	15944	16294	13.4
16300	16400	16294	16394	13.6
16400	16550	16394	16544	13.7
16550	17150	16544	17143	13.8
17150	17900	17143	17893	13.8
17900	18800	17893	18792	13.8
18800	18950	18792	18942	13.8
18950	19800	18942	19790	14.7
19800	19850	19790	19840	14.7
19850	19950	19840	19940	14.7
19950	20650	19940	20638	14.7
20650	22150	20638	22138	14.7
22150	23600	22138	23588	14.7
23600	24117	23588	24105	14.7
24117	24150	24105	24138	13.7
24150	24750	24138	24738	13.8
24750	25000	24738	24988	13.8
25000	26200	24988	26186	13.8

26200	26550	26186	26536	13.8
26550	27400	26536	27386	13.8
27400	27825	27386	27811	13.8
27825	27900	27811	27886	13.9
27900	27950	27886	27936	14
27950	28500	27936	28486	14
28500	28700	28486	28686	14

Table 38. Leak-off test drilling data of Well B2

TVD	LOT
ft	ppg
6812	11
7548	12
12909	16
24105	15.5

Table 39. MDT drilling data of Well B2

TVD	MDT
ft	ppg
28084	13.36515
28106	13.36257
28342	13.32519
28409	1.332087
28456	13.30998
28506	13.30095
28536	13.29718
28594	13.28712
27386	13.45959
26756	13.47878
25837	13.63432
24363	13.08559
26888	13.46
26950	13.44979
26980	13.44483
27004	13.4404
27031	13.43698
27281	13.48109
27296	13.47871
27361	13.46565
27406	13.45922
27423	13.45571
27580	13.44482
27746	13.42034
27682	13.43168
27603	13.44185
27812	13.40986
27866	13.40053
27964	13.38435

TVD	MDT
ft	ppg
27964	13.38435
28018	13.37613
25891	13.62497
25719	13.6575
26087	13.61067
26150	13.59943
26325	13.53666
26341	13.53386
26371	13.52794
26483	13.51064
26501	13.50729
26510	13.50574
26546	13.50062
26796	13.47206
24348	13.08926
24371	13.08566
24400	13.07999
24452	13.07663
24500	13.0874
24501	13.08568
25432	13.71439
25411	13.71854
25587	13.68564
25797	13.6425
25683	13.66556
25770	13.6477
25835	13.63549
25861	13.63062

Table 40. Casing points of Well B2

TVD	Casing
ft	in
6812	22
7548	18
12909	13 5/8
24105	9 5/8

REFERENCES

[1] Munn, M.J. , "Studies in the application of anticlinal theory of oil and gas accumulation," Economic Geology, vol. 4, pp. 141-147, 1909.

[2] Hubbert, M. K., "The theory of ground-water motion," Journal of Geology, vol. 48, pp. 785-944, 1940.

[3] Hubbert, M. K., "Entrapment of petroleum under hydrodynamic conditions," AAPG Bulletin. vol. 37, pp. 1954-2026, 1953.

[4] Hubber, M. K. and W. W. Rubey, "Role of fluid pressure in mechanics of overthrust faulting. Part 1: mechanics of fluid-filled porous solids and its application to overthrust faulting," GSA Bulletin, vol. 70, pp. 115-166 1959.

[5] Bradley, J.S., "Abnormal formation pressure," AAPG Bulletin, vol. 59, pp. 957-973, 1975.

[6] Stanescu, V., C. Carraru, and D. Varvarici, "Abnormal pressure and structure of the gas bearing reservoirs of some salt domes of the Transylvanian Depression," Bulletin of the Institute of Petroleum, Geological Gazette, Bucharest, Romania, vol. 17, pp. 239-257, 1969.

[7] North, F. K., "Petroleum geology," Boston, Allen and Unwin, 1985.

[8] Dickinson, G., "Geological aspects of abnormal reservoir pressures in Gulf Coast Louisiana," Bull. Am. Assoc. Pet. Geol., vol. 37, pp. 410-432, 1953.

[9] Terzaghi, K. and Peck, R.B., "Soil Mechanics In Engineering Practice," Wiley New York, N.Y, pp. 566, 1948.

[10] Hottman, C.E. and Johnson, R.K., "Estimation of formation pressures from log-derived shale properties," J. Pet. Technol., vol. 17, pp. 717-722, 1965.

[11] Eaton, B.A., "The effect of overburden stress on geopressure prediction logs," J. Pet. Technol., vol. 24, 1972.

[12] Eaton, B. A., and Eaton, T.L., "Fracture Gradient Prediction for the New Generation," World Oil, October 1997, pp. 93-100, 1997.

[13] Bower, G.L., "Pore Pressure Estimation From Velocity Data: Accounting for Overpressure Mechanisms Besides Undercompaction," IADC/SPE 27488, 1994.

[14] Magara, K., "Compaction and migration of fluids in miocene mudstone, Nagaoka Plain, Japan," Bull. Am. Assoc. Pet. Geol., vol. 52, pp. 2466-2501, 1968.

[15] Magara, K., "Permeability considerations in generation of abnormal pressures," Soc. Pet. Eng. J., vol. 11, pp. 236-242, 1971.

[16] Magara, K., "Thickness of removed sediments, paleopore pressure, and paleotemperature, southwestern part of Western Canada Basin." Bull. Am. Assoc. Pet. Geol., vol. 60, pp. 554-565, 1976.

[17] Magara, K., "Compaction and fluid migration: practical petroleum geology," Elsevier Scientific Publishing Company, 1978.

[18] Sawyer, D., Flemings, P., Shipp, C., and Winker, C., "Seismic geomorphology, lithology and evolution of the late Pleistocene Mars-Ursa turbidite region, Mississippi Canyon area, northern Gulf of Mexico," AAAPG Bulletin, vol. 91, No. 2, pp. 214-234, February 2007.

[19] Tuncay, K., Park, A., and Ortoleva, P., "3-D Coupled Basin Reaction Transport, and Mechanics Modeling: Applications to Fracture, Fault, and Salt Tectonic Regimes," AAPG/Datapages Discovery Series No.7, pp. 217-242, 2003.

[20] Bruce, B., and Bowers, G., "Pore pressure terminology," The Leading Edge, pp. 170-173, February 2002.

[21] Lupa, J., Flemings, P., and Tennant, S., "Pressure and trap integrity in the deepwater Gulf of Mexico," The Leading Edge, pp. 184-187, February 2002.

[22] Bower, G., "Detecting high overpressure," The Leading Edge, pp. 174-177, February 2002.

[23] Risch, D., Chowdhury, A., and Hanna, A., "Regional Depositional History of the Miocene-Pleistocene Louisiana Slope, Green Canyon-Mississippi Canyon," Transactions Of The Gulf Coast Association of Geological Societies, vol. 44, 1994.

[24] Powley, D., "Pressures and hydrogeology in petroleum basins," Earth-Science Reviews, vol. 29, pp. 215-226, 1990.

[25] Downey, M., "Evaluating Seals for Hydrocarbon Accumulations," The American Association of Petroleum Geologists, vol. 68, pp. 1752-1763, November 1984.